Stem Cell Reports
Article

ISSCR

OPEN ACCESS

Serine Racemase mediates subventricular zone neurogenesis via fatty acid metabolism

Robin Roychaudhuri,[1,4,*] Hasti Atashi,[1] and Solomon H. Snyder[1,2,3]
[1]Department of Neuroscience, Johns Hopkins University School of Medicine, Baltimore, MD 21205, USA
[2]Department of Psychiatry and Behavioral Sciences, Johns Hopkins University School of Medicine, Baltimore, MD 21287, USA
[3]Department of Pharmacology and Molecular Sciences, Johns Hopkins University School of Medicine, Baltimore, MD 21287, USA
[4]Present address: University of Maryland School of Medicine, Department of Obstetrics, Gynecology and Reproductive Sciences, Center for Birth Defects, Baltimore, MD 21201, USA
*Correspondence: robinroychaudhuri@gmail.com
https://doi.org/10.1016/j.stemcr.2023.05.015

SUMMARY

The adult subventricular zone (SVZ) is a neurogenic niche that continuously produces newborn neurons. Here we show that serine racemase (SR), an enzyme that catalyzes the racemization of L-serine to D-serine and vice versa, affects neurogenesis in the adult SVZ by controlling *de novo* fatty acid synthesis. Germline and conditional deletion of SR (nestin precursor cells) leads to diminished neurogenesis in the SVZ. Nestin-cre+ mice showed reduced expression of fatty acid synthase and its substrate malonyl-CoA, which are involved in *de novo* fatty acid synthesis. Global lipidomic analyses revealed significant alterations in different lipid subclasses in nestin-cre+ mice. Decrease in fatty acid synthesis was mediated by phospho Acetyl-CoA Carboxylase that was AMP-activated protein kinase independent. Both L- and D-serine supplementation rescued defects in SVZ neurogenesis, proliferation, and levels of malonyl-CoA *in vitro*. Our work shows that SR affects adult neurogenesis in the SVZ via lipid metabolism.

INTRODUCTION

Adult neurogenesis is the production of new neurons in the subventricular zone (SVZ) of the lateral ventricles and the sub granular zone of the hippocampus in the brain (Kempermann, 2006; Ming and Song, 2011; Tong and Alvarez-Buylla, 2014). Newborn neurons in the SVZ migrate along the rostral migratory stream (RMS) and eventually differentiate into olfactory bulb (OB) interneurons feeding the precursor cell population (Lim and Alvarez-Buylla, 2016). Recent work has shown that adult neurogenesis depends on metabolic control of fatty acid synthesis (Knobloch, 2017; Knobloch et al., 2013). Defects in fatty acid metabolism play a crucial role in the quiescent and proliferative behavior of neural progenitor cells (Clemot et al., 2020; Knobloch et al., 2017). Serine racemase (SR) is a pyridoxal phosphate (PLP)-dependent enzyme that synthesizes D-serine from L-serine and vice versa (Wolosker et al., 1999a, 1999b). D-serine functions as a neurotransmitter during brain development (Schell et al., 1997). SR-deficient mice show NMDA receptor hypofunction and is considered a model for schizophrenia (Balu et al., 2013; Basu et al., 2009); however, little is known of D-serine's functions outside the NMDA receptor. D-serine regulates proliferation and differentiation of neural stem cells (NSCs) from postnatal mouse forebrain (Huang et al., 2012). D-serine has been implicated in adult hippocampal neurogenesis, with exogenous treatment of D-serine increasing the density of NSCs, transit amplifying progenitors and increased survival of newborn neurons (Sultan et al., 2013). We investigated the metabolic role of SR in NSCs from the adult SVZ. We hypothesized that SR may influence metabolism in the SVZ due to L- and D-serine synthesis and transport via the astrocyte-neuron shuttle (Wolosker et al., 2017; Ehmsen et al., 2013).

Using lipidomic analysis and biochemical approaches, we show that the SVZ of nestin-cre+ mice have significant alterations in the different classes of lipids, decreased expression of fatty acid synthase (FASN) and malonyl-CoA, a precursor for *de novo* fatty acid synthesis. Our work also shows that SR mediates its effects in the SVZ via activation of acetyl-CoA carboxylase (ACC). SR may influence lipid metabolism by regulating astrocytic L-serine and consequently neuronal D-serine synthesis in NSCs. These findings may have therapeutic implications in the treatment of disorders of adult neurogenesis like schizophrenia and Alzheimer's disease (Le Douce et al., 2020; Moreno-Jimenez et al., 2019; Schoenfeld and Cameron, 2015; Yun et al., 2016).

RESULTS

Lack of SR leads to defects in adult SVZ neurogenesis and proliferation

SR is a PLP-dependent enzyme, which racemizes D-serine in neurons from L-serine in astrocytes (Wolosker et al., 1999b, 2017). We determined neurogenesis in the SVZ of adult wild-type (WT) and $SR^{-/-}$ mice (Figures 1A, 1B, S1A and S4D). We monitored BrdU incorporation in age-matched WT and $SR^{-/-}$ mice for 14 days (Doetsch et al., 1999). Our data showed significantly reduced incorporation of BrdU

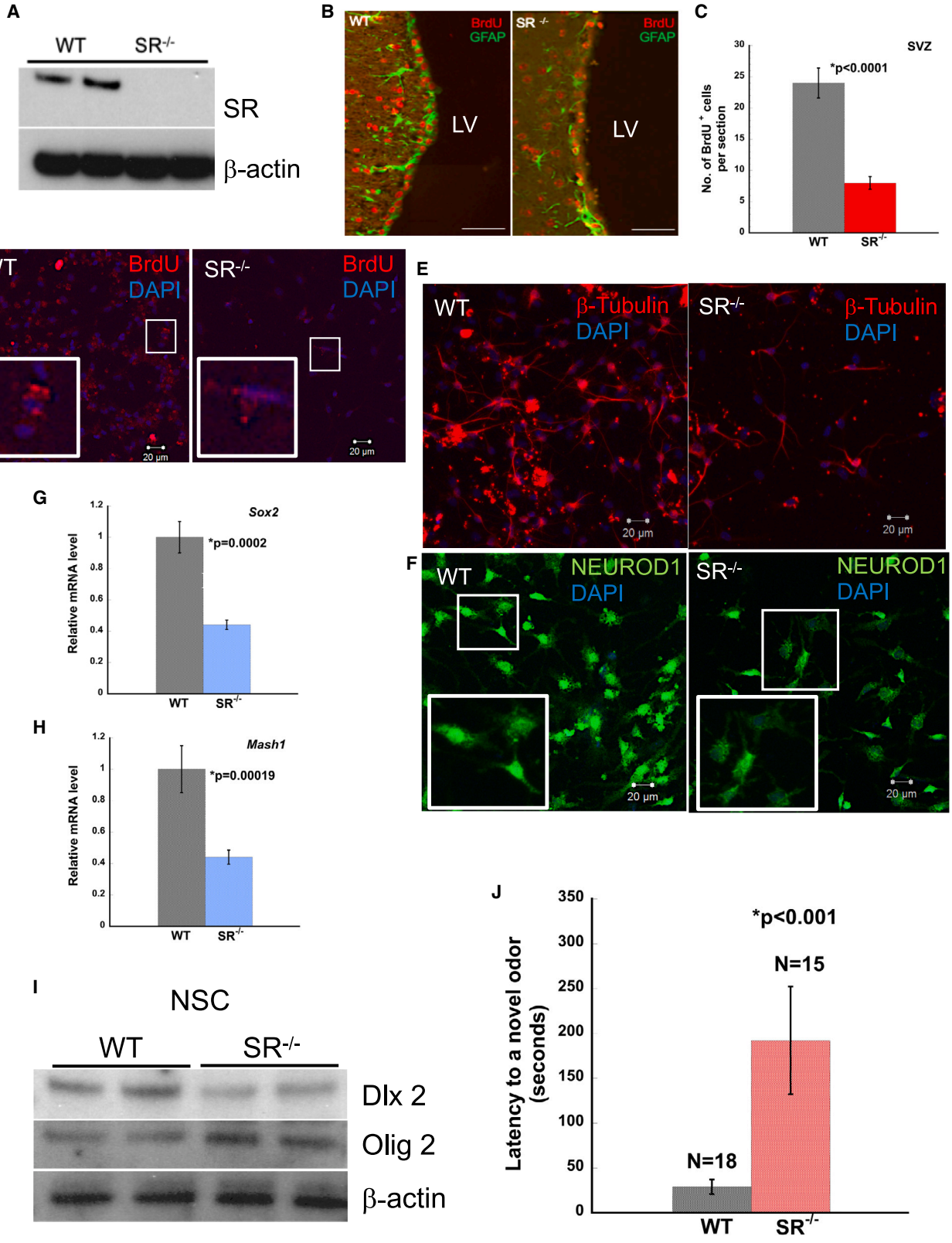

(legend on next page)

in $SR^{-/-}$ mice (Figures 1B and 1C). Quantitative analysis showed 4-fold reduction in BrdU-positive cells in $SR^{-/-}$ mice (Figure 1C). Glial fibrillary acidic protein (GFAP)-positive staining (mature astrocytes) was decreased in the SVZ of $SR^{-/-}$ mice (Figure 1B).

The neuroblast assay serves as an *in vitro* model of neurogenesis (Azari and Reynolds, 2016; Azari et al., 2012). To determine neurogenesis *in vitro*, we performed the neuroblast assay. NSCs were isolated from the SVZ of age-matched adult WT and $SR^{-/-}$ mice and grown as adherent monolayer cultures for 10–12 days (Walker and Kempermann, 2014). After 4 days in media with reduced and eventually no growth factors, neuroblasts were observed above a layer of astrocytes (Figure S2A) (Azari and Reynolds, 2016). We examined BrdU incorporation in NSCs as an indicator of cell division. BrdU incorporation in NSCs from WT and $SR^{-/-}$ SVZ showed 4-fold lower incorporation in $SR^{-/-}$ (*$p = 0.0084$) (Figures 1D and S2D).

Neuroblasts (type A cells) migrate rostrally and differentiate to OB interneurons. We determined the expression of β-III Tubulin (marker for immature neurons) and NEUROD1 (marker for neuroblasts). β-III Tubulin staining in NSCs was reduced in $SR^{-/-}$ mice (Figure 1E). Quantitative analysis showed 5-fold reduction of β-III tubulin positive staining in $SR^{-/-}$ mice (*$p < 0.001$) (Figure S2B). A similar trend was observed with NEUROD1 (*$p < 0.001$) (Figures 1F and S2C). We examined the differentiation of NSCs to astrocytes and neurons. GFAP expression was reduced in $SR^{-/-}$ mice (Figure S1C). NEUN expression (marker for newborn post mitotic neurons) was also reduced in $SR^{-/-}$ NSCs (Figure S1D). Gene expression for markers of proliferation in the OB, *Sox2*, and *Mash1* showed 2-fold reduction in $SR^{-/-}$ mice (Figures 1G and 1H). To substantiate our findings, we determined and observed reduced expression of DLX2 in $SR^{-/-}$ NSCs (Figures 1I and S6A). We also observed increased expression of OLIG2 in $SR^{-/-}$ NSCs (Figures 1I and S6B), suggesting a propensity for oligodendrocyte differentiation (Wang et al., 2020). We determined the expression of Ki67 in primary neurons derived from NSCs. $SR^{-/-}$ neurons expressed 2-fold lower levels of Ki67 (Figure S1B). To determine the effects of SVZ neurogenesis on olfactory behavior, we performed olfactory behavior test in age-matched WT and $SR^{-/-}$ mice (Witt et al., 2009). In the novel odor test, we determined the amount of time the mice spent locating and sniffing the novel odor. WT mice spent a shorter time exploring and sniffing the novel odor compared with $SR^{-/-}$ mice that took approximately eight times longer (*$p < 0.001$) (Figure 1J). Collectively, these results show that $SR^{-/-}$ mice have defects in adult SVZ neurogenesis and proliferation *in vitro* and *in vivo*.

Conditional deletion of SR leads to defects in adult SVZ neurogenesis and proliferation

We conditionally deleted *Srr* in nestin precursor cells (nestin-cre+) to elucidate its function in neural progenitor cells (Bernal and Arranz, 2018; Wiese et al., 2004). Our rationale was 2-fold first, D-serine the product of *Sr* may control neuronal development and generation of newborn neurons (Schell et al., 1997). Second, neuronal D-serine synthesis dependent on astrocytic L-serine may influence proliferation and metabolic homeostasis. SR expression was reduced in the brains of nestin-cre+ mice compared with age-matched $SR^{flox/flox}$ (Figure 2A). We ascertained levels of neurogenesis in the SVZ of adult mice by monitoring BrdU incorporation (Doetsch et al., 1999). BrdU imaging showed 1.5-fold reduced incorporation in nestin-cre+ mice (Figures 2B and 2C). Expression of Ki67, a proliferative marker for early adult neurogenesis, showed approximately 2-fold decreased expression in the SVZ of nestin-cre+ mice (Figures 2D and 2E) (Kee et al., 2002).

We monitored expression of MCM2 (DNA Replication Licensing Factor; marker for proliferation of mitotic progenitor cells) in the SVZ. We observed approximately 3-fold reduction of MCM2 expression in nestin-cre+ mice (Figures 2F and S7F). Prominin 1 is a marker for NSCs in the adult SVZ (Faigle and Song, 2013). Prominin 1 expression was reduced 4-fold in nestin-cre+ mice (Figures 2G and S7G). We determined expression of mCD24 (glycosylphosphatidyl inositol membrane anchored glycoprotein) that regulates the proliferation of committed neuronal precursors in the SVZ and is a negative regulator of cell proliferation (Belvindrah et al., 2002; Doetsch et al., 1999). Nestin-cre+ mice showed 3-fold higher expression of mCD24 (Figures 2J and S4E). SRY-box 2 (SOX-2) is a transcription

Figure 1. Lack of Serine Racemase leads to defects in adult SVZ neurogenesis and proliferation *in vivo*

(A) Expression of SR in WT and $SR^{-/-}$ mice SVZ lysates.

(B) WT and $SR^{-/-}$ SVZ lateral ventricle showing BrdU incorporation (red) and GFAP expression (green). Scale bar, 100 μm.

(C) Quantitative estimation of BrdU+ cells.

(D–H) BrdU incorporation in NSC from WT and $SR^{-/-}$ SVZ. Inset shows incorporation of BrdU in NSCs (red). Expression of (E) β-III Tubulin and (F) NEUROD1 in NSCs from WT and $SR^{-/-}$ mice after differentiation. Relative mRNA levels of (G) *Sox2* and (H) *Mash1* in olfactory bulb of WT and $SR^{-/-}$ mice. Error bars represent SD. Data are representative of three independent experiments and tissues pooled from n = 5–6 mice/experiment.

(I) Expression of DLX2 and OLIG 2 in NSC lysates.

(J) Mouse olfactory behavior test in age-matched WT and $SR^{-/-}$ mice. N = number of mice.

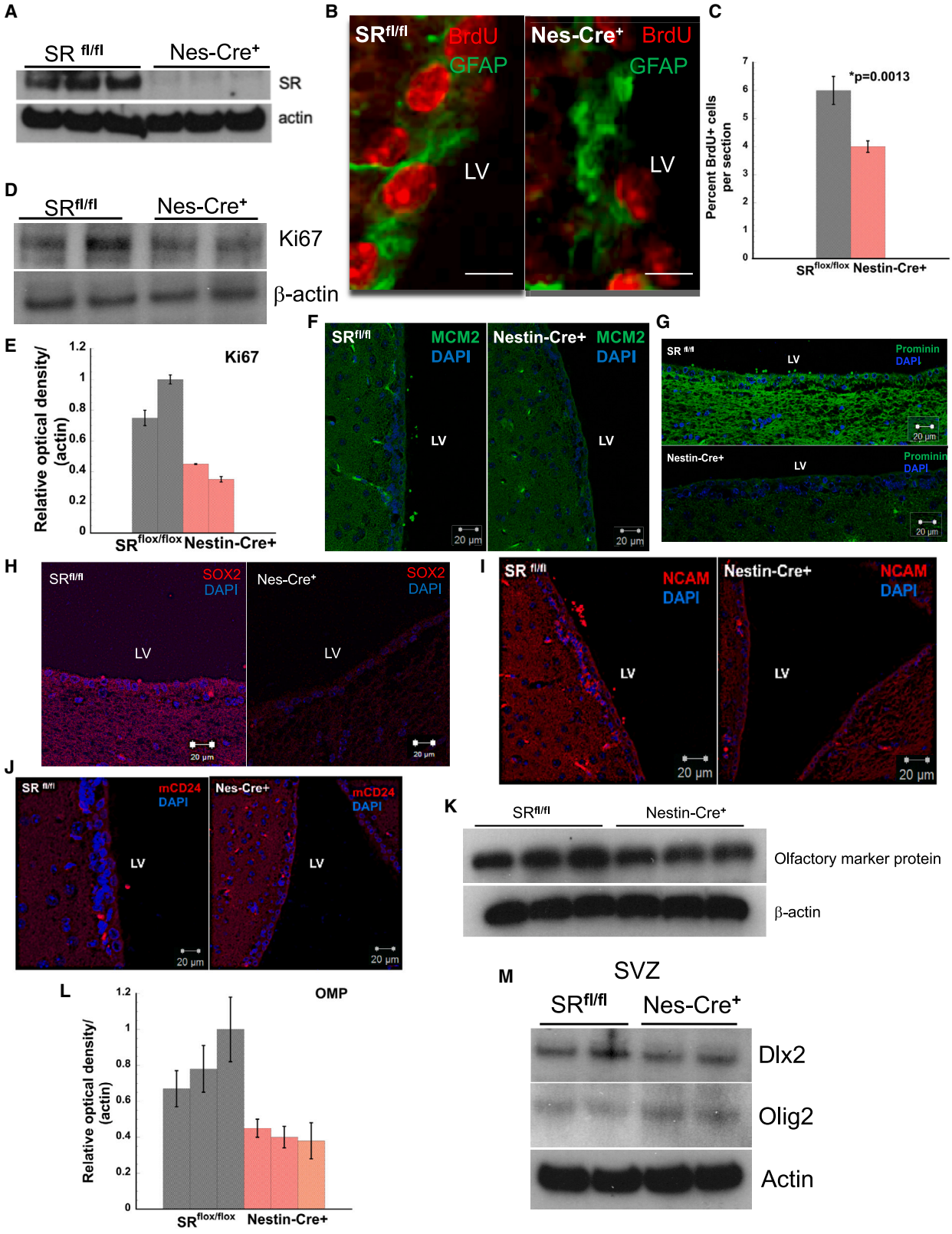

(legend on next page)

factor essential for self-renewal and differentiation of neural progenitor cells (Pevny and Nicolis, 2010). SOX-2 expression in the SVZ was 3-fold lower in nestin-cre+ mice (Figures 2H and S7I). Expression of polysialylated specific antigen-neuronal cell adhesion molecule (PSA-NCAM) (Figures 2I and S7H) and GFAP (Figure S5C) was 6- and 5-fold lower in nestin-cre+ mice. We also observed reduced PSA-NCAM expression along the RMS in nestin-cre+ mice (Figure S5B).

We determined expression of olfactory marker protein (OMP) present on olfactory receptor neurons and observed 2-fold decrease in nestin-cre+ mice suggesting defects in adult SVZ neurogenesis (Figures 2K and 2L). We observed reduced expression of proliferation marker DLX2 in the SVZ of nestin-cre+ mice (Figures 2M and S6C). Expression of OLIG2 (cell fate determination of motor neurons and oligodendrocytes) was increased in nestin-cre+ mice (Figures 2M and S6D), suggesting that conditional deletion of *Srr* may increase propensity for oligodendrocyte differentiation (Wang et al., 2020). Collectively our data show that nestin-cre+ mice have defects in SVZ neurogenesis and proliferation and support the data with $SR^{-/-}$ mice (Figures 1B and 1C).

SR alters L-serine and *de novo* fatty acid synthesis in the SVZ of nestin-Cre+ mice

L-serine synthesized by astrocytes regulates neuronal development (Furuya et al., 2000; Kalhan and Hanson, 2012; Mitoma et al., 1998; Reid et al., 2018). SR racemizes L-serine and D-serine (Wolosker et al., 1999b, 2017). We hypothesized that deletion of *Srr* may have metabolic implications for neuronal development. L-serine synthesis is regulated by phosphoglycerate dehydrogenase (PGDH) and phosphoserine phosphatase (PSPH) via the phosphorylated pathway (Fell and Snell, 1988; Snell and Fell, 1990; Yamasaki et al., 2001). STRING analysis followed by k means clustering shows that SR interacts with PSPH and PHGDH in both mice and humans (Figures S6E and S6F). We determined expression of *Pgdh* and *Psph* in the SVZ and observed decreased expression of both enzymes in nestin-cre+ mice (Figures 3A, S7J, and S7K). Relative mRNA levels showed more than 50% reduction in enzymes in nestin-cre+ mice (Figure 3B). Protein expression was also decreased in the SVZ of nestin-cre+ mice (Figure 3C), supporting a consistent trend (Ehmsen et al., 2013). To determine if 0.4 mM L-serine in the culture media alters expression of PGDH and PSPH, we determined their expression in WT and $SR^{-/-}$ NSCs. We found decreased expression of both enzymes in $SR^{-/-}$ NSCs (Figure 3E). FASN controls the synthesis of fatty acids by synthesizing palmitate from acetyl- and malonyl-CoA. We observed 3-fold reduction in FASN expression in nestin-cre+ SVZ (Figures 3D and S7E). In whole brain we observed approximately 50% lower FASN expression in nestin-cre+ mice (Figures S2E and S2F). To confirm, we estimated FASN levels using ELISA. We found lower expression in the brain and significantly lower levels in the SVZ of nestin-cre+ mice (Figures 3F and 3H). These data strongly suggest that nestin-cre+ mice have defects in *de novo* fatty acid synthesis. *Spot 14* (thyroid hormone responsive spot14) is a regulator of *de novo* lipogenesis and is involved in proliferation of adult NSCs (Knobloch et al., 2014). It negatively regulates malonyl-CoA, an essential substrate for FASN in *de novo* lipogenesis. We observed higher expression of SPOT 14 in nestin-cre+ mice (Figures 3G and S5A). MIG12 (Midline-1-Interacting G12 like protein) complexes with SPOT14 to regulate ACC (Knobloch et al., 2013; Park et al., 2013). We determined mRNA levels of *Mig12* in the SVZ and observed 10-fold higher expression in nestin-cre+ mice (Figure 3I). We estimated levels of malonyl-CoA in the SVZ and observed that $SR^{flox/flox}$ levels were 1,500 ng/mL, while nestin-cre+ levels were 1,200 ng/mL (*p = 0.054 relative to $SR^{flox/flox}$ control) (Figure 3J). Levels of malonyl-CoA suggest that *de novo* lipogenesis fueled by FASN and its substrate is impaired in nestin-cre+ mice.

Global lipidomic profile altered in the SVZ of adult $SR^{flox/flox}$ and Nestin-Cre+ mice

Recent evidence implicates lipids in stem cell development and proliferation (Knobloch, 2017; Knobloch et al., 2013; Knobloch and Jessberger, 2017; Lodhi et al., 2011). Our rationale stems from serine metabolism regulating ceramide and sphingolipid levels including cell proliferation (Furuya et al., 2000; Gao et al., 2018; Kalhan and Hanson,

Figure 2. Conditional deletion of *Srr* leads to defects in adult SVZ neurogenesis and proliferation

(A) Expression of SR in $SR^{flox/flox}$ and nestin-cre+ mice brain.

(B) BrdU incorporation (red) and GFAP expression (green) in the SVZ of $SR^{flox/flox}$ and nestin-cre+ mice. Scale bar, 100 μm.

(C) Quantitative estimation of BrdU+ cells counted in different high-powered fields per section. n = 4–5 mice.

(D) Expression of Ki67 in SVZ.

(E–J) Densitometric analysis of blot in (D). Expression of NSC and proliferation markers (F) MCM2, (G) Prominin, (H) SOX2, (I) NCAM, and (J) mCD24 in $SR^{flox/flox}$ and nestin-cre+ mice. Scale bar, 20 μm.

(K) Expression of OMP in SVZ.

(L) Densitometry of OMP blot.

(M) Expression of DLX2 and OLIG 2 in SVZ.

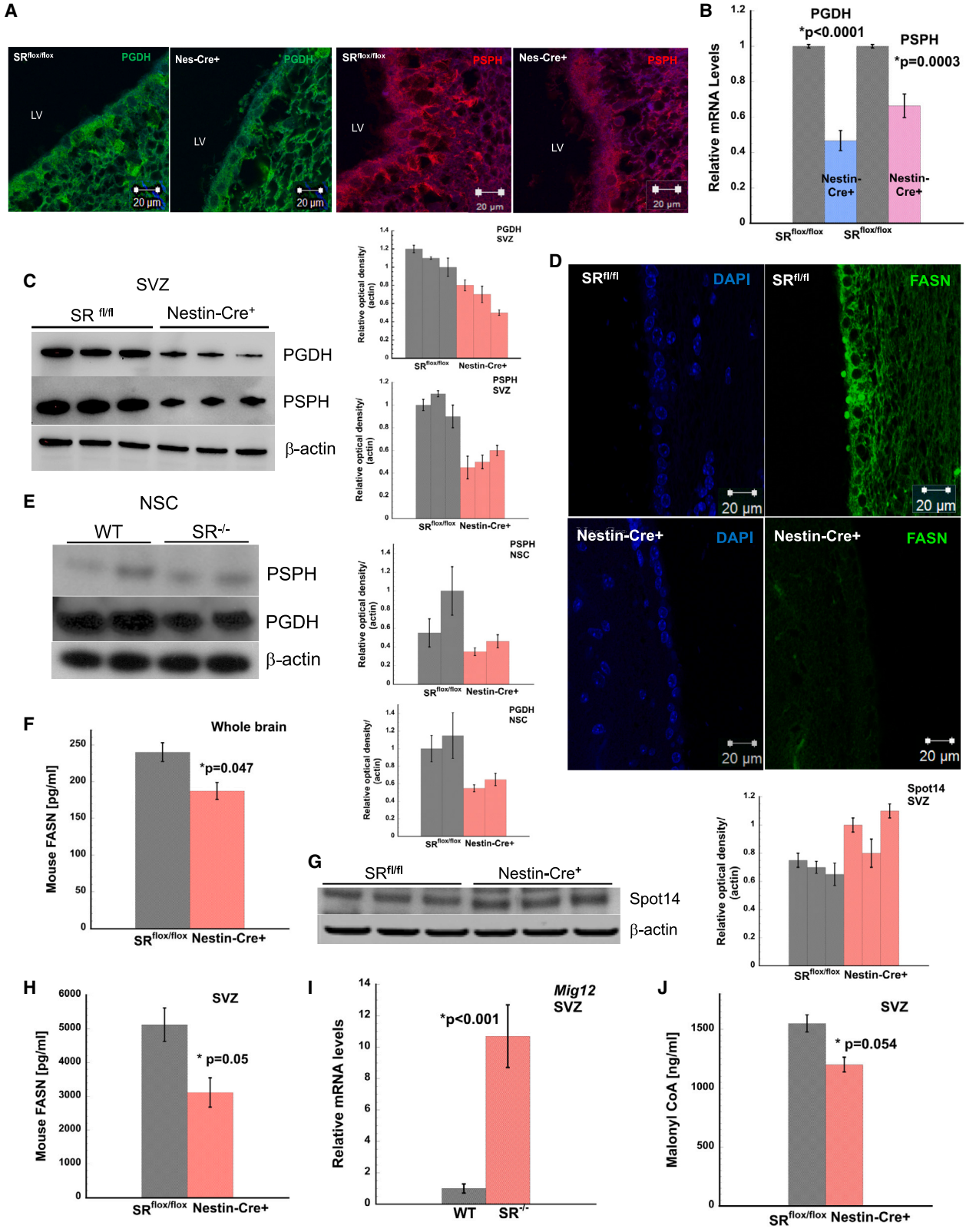

(legend on next page)

2012). We performed global lipidomic analysis in SVZ of age-matched $SR^{flox/flox}$ and nestin-cre+ mice by lipid extraction followed by UPLC-MS/MS identification (Figure 4A). Volcano plot with fold change (mean nestin-cre+/mean $SR^{flox/flox}$) $\geq$1.5 or $\leq$0.667 and p value adjusted for false discovery rate <0.05 (criteria for significance), resulted in 184 lipids with fold change $\geq$1.5 (red) and 312 lipids with fold change $\leq$0.667 (blue) (Figure 4B). The different lipid classes were identified in three tiers of MS/MS analysis (Figure 4C). In tier one (404 features with MS/MS match score threshold of 500), two (146 features with MS/MS match score threshold of 100), and three (remaining features in the lipidome database for putative mass match) with a mass error threshold of 5.0 mDa were identified. Out of 8,648 unique features detected, 5,262 features (60.6%) were identified. The summed intensities showed good stability in data acquisition (Figure S4C). Thirteen internal standards were detected in positive ionization and 12 internal standards in negative ionization (Figure 4D). The mass error was less than 2.8–3.0 ppm. Heatmap of the lipidomic analysis with the top 50 lipids (ranked by p value) is shown in Figure 4E. The heatmap data show substantial downregulation of highly ranked lipids (by p value) in the SVZ of nestin-cre+ mice. Out of the top 50 lipids, 37 were downregulated and 13 upregulated in nestin-cre+ mice compared with $SR^{flox/flox}$. The identified lipids are listed in Tables S4 and S5. Partial least squares-discriminant analysis with variable importance in prediction scores of 15 of the most important lipids (Figure 4F, Table S1) identified a diverse group of lipids that were significantly altered. A caveat of nestin-cre mouse strain is the presence of metabolic phenotypes (Declercq et al., 2015; Harno et al., 2013). Nestin-cre strain show lower levels of growth hormone, impaired insulin sensitivity, and impaired glucose levels on a high-fat diet. In order to rule out confounding effects, we estimated plasma glucose and insulin levels in age-matched $SR^{flox/flox}$ and nestin-cre+ mice fed a normal diet. Our data show no difference in plasma glucose levels in $SR^{flox/flox}$ and nestin-cre+ mice (Figure 4G). Total brain and SVZ insulin showed no differences (Figures 4H and 4J). We determined brain insulin levels in age-matched WT and $SR^{-/-}$ mice (background on which $SR^{flox/flox}$ mice were generated) to rule out mice background effects. Our data showed no difference in brain insulin in WT and $SR^{-/-}$ mice (Figure 4I). We determined expression of growth hormone in the SVZ and found no change in WT and $SR^{-/-}$ mice except a modest decrease in nestin-cre+ mice (Figure 4K). Control experiments suggest that the metabolic differences in our work are due to conditional deletion of *Srr*. The lipidomics data clearly highlight major differences among the different lipid classes in the SVZ of nestin-cre+ mice.

Major lipid classes altered in the SVZ of nestin-cre+ mice

Global lipidomic analysis in the SVZ of nestin-cre+ and $SR^{flox/flox}$ mice by UPLC-MS/MS showed significant alterations in the different classes of lipids. We plotted lipidomics data as fold change relative to $SR^{flox/flox}$ (significant). The different lipid classes were fatty acid conjugates, sphingomyelins, phosphatidylcholine, phosphatidic acid, ceramides, sterols, carnitine, tri, di, and monoacylglycerols, hexosylceramides, and lysophosphatidic acid. Fatty acid conjugates are polyunsaturated fatty acids with conjugate double bonds. Out of the three fatty acid conjugates, two showed modest decrease in nestin-cre+ while FA 12:0; O4 showed 2-fold higher levels in nestin-cre+ mice (Figure S3A, Table S2). L-serine availability affects the synthesis of ceramides, sphingomyelin, and phosphatidylserine (Esaki et al., 2015; Gao et al., 2018). Our data show reduction by >50% in all the sphingomyelin species identified (Figure S3B, Table S2). Most notable decrease was seen in sphingomyelin 38:1; O2 in nestin-cre+ mice. Phosphatidylcholine synthesis was significantly reduced (>40%) in the SVZ of nestin-cre+ mice (Figures S3C, S4A and Table S2). Phosphatidic acid (low abundance phospholipid) showed increases ($\geq$2-fold) in PA 8:0_25:0, PA 36:1 and PA 19:2_19:2 and decrease ($\geq$2-fold) in the remaining molecules in nestin-cre+ mice

Figure 3. Serine Racemase alters L-serine and *de novo* fatty acid synthesis in the SVZ of nestin-cre+ mice

(A) Expression of PGDH (green) and PSPH (red) in the SVZ of $SR^{flox/flox}$ and nestin-cre+ mice. Scale bar, 20 μm.

(B) Relative mRNA levels of *Pgdh* and *Psph*. Data are representative of three independent experiments. Tissues were pooled from n = 5–8 mice.

(C) Expression of PSPH and PGDH in SVZ.

(D) Expression of mouse FASN in SVZ. Scale bar, 20 μm.

(E) Expression of PSPH and PGDH in NSC lysates.

(F) Mouse FASN expression in whole brain homogenates. *p = 0.047 relative to $SR^{flox/flox}$.

(G) Expression of SPOT14 in SVZ.

(H) Expression of mouse FASN in SVZ. *p = 0.05 relative to $SR^{flox/flox}$.

(I) mRNA levels of SPOT14 regulator *Mig12* in SVZ of WT and $SR^{-/-}$ mice.

(J) Estimation of malonyl-CoA in SVZ by ELISA. *p = 0.054 relative to $SR^{flox/flox}$. Error bars are SD. Data are representative of three independent experiments. Tissues were pooled from n = 5–8 mice per experiment.

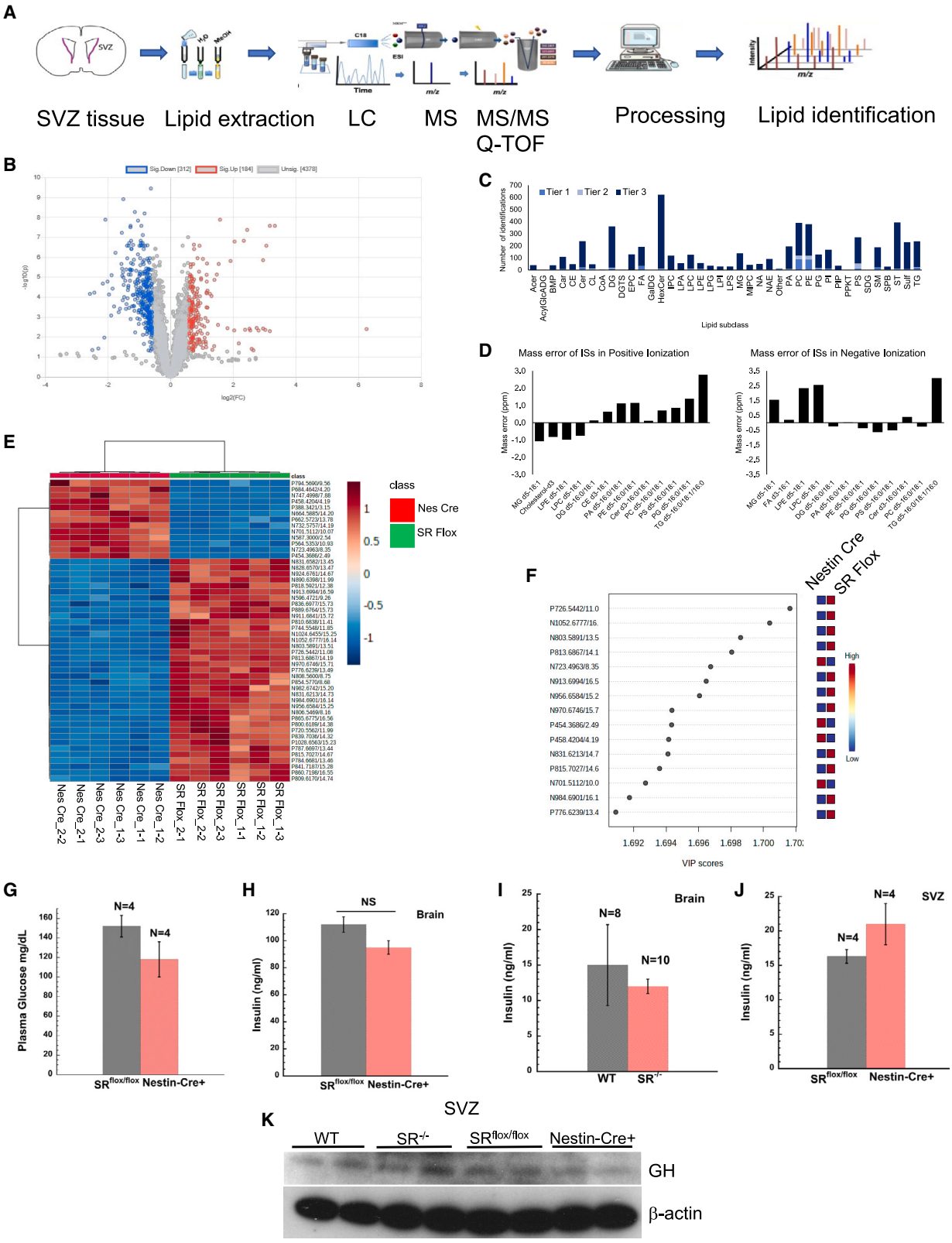

(legend on next page)

(Figure S3D, Table S2). All identified ceramides in our screen showed approximately 40% or higher reduction in nestin-cre+ mice (Figure S3E, Table S2). Sterol expression was consistently increased above 3-fold in all the identified species with the exception of ST 22:1; O4 whose expression was down 10-fold in nestin-cre+ mice (Figure S3F, Table S2). Carnitine (a branched non-essential amino acid) expression was reduced by 50% for three of the identified four species with the exception of CAR 24:1; O2, which was increased 2-fold in nestin-cre+ mice (Figure S3G, Table S2). Both tri and diacylglycerols (synthesized from fatty acyl-CoA and glycerol 3 phosphate) were reduced by 50% or more in nestin-cre+ mice with the exception of TG 70:3, TG 75:4 (Figure S3H, Table S2) and DG 34:1 and DG O-24:1 (Figure S3I, Table S2) that were increased ($\geq$2.5-fold). Monoacylglycerols were increased 2-fold in nestin-cre+ mice (Figure S3J, Table S2). Hexosylceramides are sphingolipids with hexose ring attached to a ceramide. Nestin-cre+ mice showed consistent downregulation ($\geq$40%) in all the hexosylceramide molecules identified (Figure S3K, Table S2). Lysophosphatidic acid (a bioactive phospholipid produced during cell membrane synthesis) showed bidirectional trends with LPA 30:2 and LPA 32:3 being reduced 2-fold and LPA O-18:3, LPA O-22:3 and LPA O-26:3 increased more than 5-fold in nestin-cre+ mice (Figure S3L, Table S2). Our lipidomic screen showed substantial alterations in most lipid classes in the SVZ of nestin-cre+ mice.

Non-AMPK-dependent ACC control of fatty acid metabolism in nestin-cre+ SVZ

ACC is a regulator of *de novo* fatty acid synthesis (Garcia and Shaw, 2017; Steinberg et al., 2006). We observed increased activation of phosho-ACC (Ser79) in nestin-cre+ mice (Figures 5B and 5E). AMP-activated protein kinase (AMPK) is a cellular sensor of nutrient availability and ATP. It controls overall cellular lipid metabolism through direct phosphorylation of ACC1 and ACC2 at Ser 79, suppressing fatty acid synthesis and simultaneously promoting fatty acid oxidation by relieving suppression of carnitine palmitoyl transferase 1 (CPT1) (Gonzalez et al., 2020; Garcia and Shaw, 2017). We observed more than 2-fold increased expression of AMPK (α) in SVZ of nestin-cre+ mice (Figures 5A and 5C). Expression of *p*-AMPK (Thr172) levels were, surprisingly, 5-fold lower in nestin-cre+ SVZ, suggesting a non-AMPK-dependent phosphorylation of ACC (Figures 5B and 5D). Based on the observed trends in *de novo* fatty acid synthesis, we determined expression of key genes in the synthesis and β-oxidation pathways. *Citrate lyase* (*Cl*) converts citrate from carbohydrate metabolism to acetyl-CoA. We observed an 8-fold increase in *Cl* mRNA expression in nestin-cre+ mice (Figure 5G). CPT1a is a key rate-limiting enzyme in long chain fatty acid oxidation and its activity is negatively regulated by malonyl-CoA. We observed approximately 500-fold increase in *Cpt1a* mRNA expression in nestin-cre+ SVZ (Figure 5G). ACC1 catalyzes the biotin dependent irreversible carboxylation of acetyl-CoA to malonyl-CoA, which serves as a key precursor in fatty acid synthesis. Our data showed 8-fold downregulation of *Acc1* and 4-fold upregulation of *Spot14* in the SVZ of nestin-cre+ mice (Figure 5G). We determined mRNA levels of key genes involved in the β-oxidation pathway. Malonyl-CoA decarboxylase (*Mcd*), which converts malonyl-CoA to acetyl-CoA, was downregulated by 50% in nestin-cre+ mice (Figure 5F). Hydroxyacyl-CoA (*HaCoA*) dehydrogenase, which is involved in β-oxidation of hydroxyacyl-CoA to oxoacyl-CoA, was elevated 30-fold in nestin-cre+ mice (Figure 5F). Enoyl-CoA Hydratase (*Ech*) catalyzes the hydration of a double bond between the second and third carbon atoms on 2-*trans*/*cis* enoyl-CoA thioester to produce β-hydroxyacyl-CoA thioester. We observed >8-fold expression of *Ech* in the SVZ of nestin-cre+ mice (Figure 5F). Collectively, these data suggest that SR may alter serine synthesis and availability, compromising the *de novo* fatty acid synthesis pathway. A concomitant increase in β-oxidation pathway may compensate for energy production in the SVZ of nestin-cre+ mice (Figure 5H).

Figure 4. Global lipidomic profile in the SVZ of nestin-cre+ mice

(A) Schematic of lipidomics workflow.

(B) Parametric volcano plot showing fold change against p value adjusted for false discovery rate. Blue circles indicate downregulation (312 lipids), red indicates upregulation (184 lipids) of lipids. Unassigned lipids are shown in gray.

(C) Lipid identification tier. In tier 1 (404 features), 2 (146 features), and 3 (remaining features).

(D) Mass error of internal standards.

(E) Heatmap of top 50 lipids ranked by p value.

(F) Plot shows partial least squares-discriminant analysis with variable importance in prediction scores of 15 most important lipids.

(G) Plasma glucose levels in $SR^{flox/flox}$ and nestin-cre+ mice.

(H and I) Insulin concentration (ng/mL) in mice whole brain homogenates.

(J) Insulin concentration (ng/mL) in mice SVZ homogenates. Error bars represent SD. NS = nonsignificant.

(K) Expression of growth hormone in mice SVZ. Error bars represent SD. Data are representative of three independent experiments. Tissues were pooled from n = 5–8 mice per experiment. For SVZ lipidomics, each genotype comprised tissues from 5 to 8 mice and injections in triplicate (see method for details).

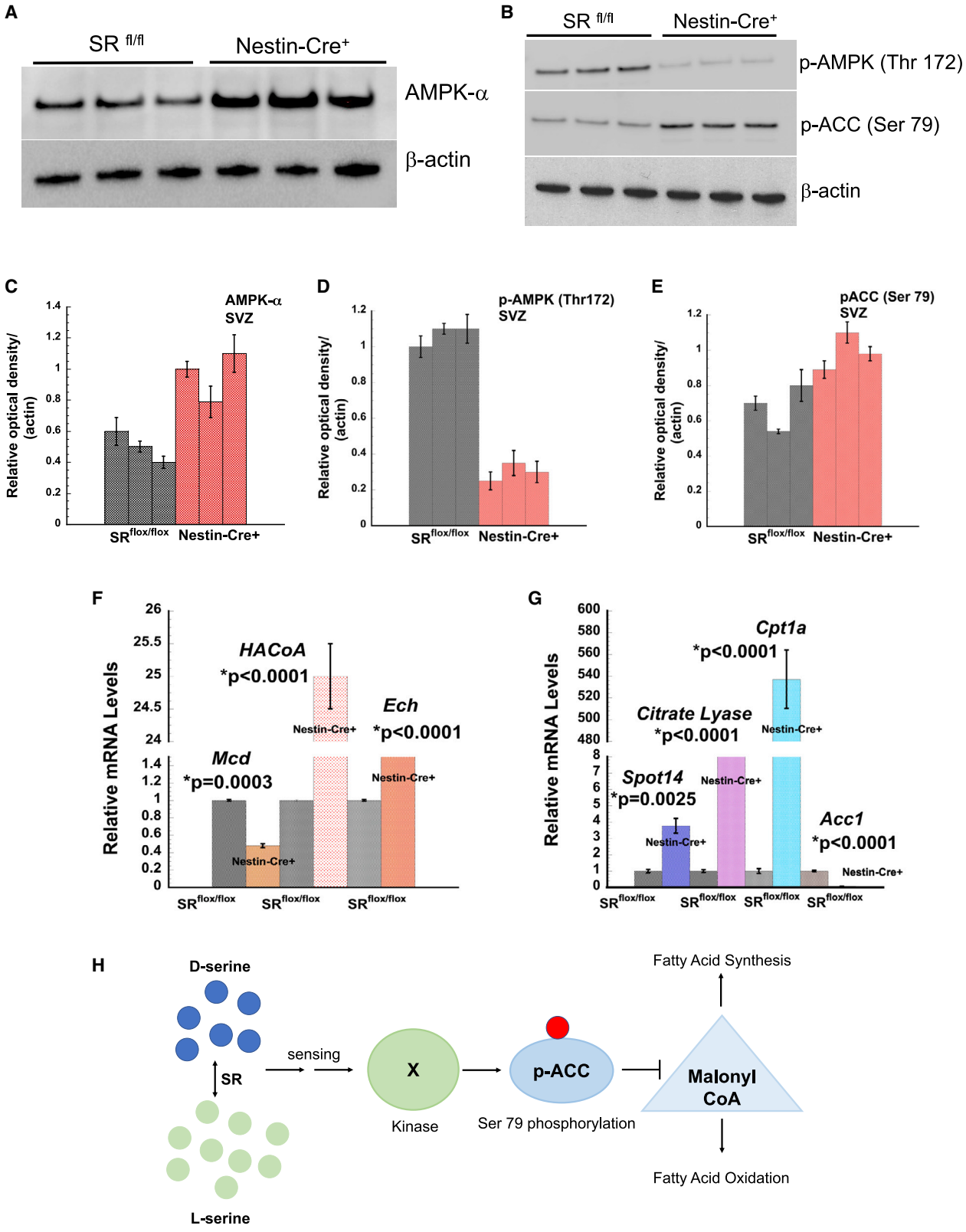

(legend on next page)

L- and D-serine rescue defects in adult SVZ neurogenesis and proliferation *in vitro*

In order to rescue defects in adult SVZ neurogenesis and proliferation in nestin-cre+ and $SR^{-/-}$ mice, we performed experiments in adherent NSCs treated with exogenous L-serine (0.6 mM) and D-serine (0.1 mM) individually and in an equimolar racemic mixture (0.1 mM each). Since neurobasal media contains basal L-serine concentration of 0.4 mM, and no D-serine, we used L-serine at a concentration of 0.6 mM. Control was media containing 0.4 mM basal L-serine with no exogenous L- and/or D-serine. We determined incorporation of BrdU in WT and $SR^{-/-}$ NSCs. $SR^{-/-}$ NSCs show significantly reduced incorporation of BrdU (Figure 6A). However, exogenous L- and D-serine increased the number of proliferating cells incorporating BrdU in $SR^{-/-}$ NSCs (Figures 6B, 6C, 6F). L- and D-serine treatment showed comparable BrdU incorporation in $SR^{-/-}$ NSCs. We also performed rescue of SOX2 in NSCs and observed lower expression of SOX2 in $SR^{-/-}$ NSCs (Figure 6D). Treatment with equimolar L- and D-serine, showed increased expression of SOX2 in both WT and $SR^{-/-}$ NSC (Figures 6D and S7B). We observed decreased NEUN expression in $SR^{-/-}$ control NSCs, but upon treatment with equimolar mixture of L- and D-serine, NEUN expression was higher than WT. We also observed that treated WT NSCs showed increased NEUN expression compared with control (Figures 6E and S7A). Nestin-cre+ mice showed increased expression of AMPK-α (Figure 5A). To determine if L- and/or D-serine alters levels of AMPK-α, we determined its expression in a rescue experiment. $SR^{-/-}$ NSCs grown in presence of L- and D-serine (0.6 mM and 0.1 mM, respectively) showed decreased expression of AMPK-α compared with untreated controls, indicating that AMPK-α expression is regulated by L- and D-serine. Interestingly, D-serine appeared to have a more potent effect on AMPK-α expression compared with L-serine (Figure 6G).

L- and D-serine rescue defects in *de novo* fatty acid synthesis and differentiation

To determine if L- and D-serine regulate PSPH, we treated NSCs with L- and D-serine (0.6 mM and 0.1 mM, respectively). Expression of PSPH was decreased in $SR^{-/-}$ NSCs (Figure 7C). Treatment with D-serine showed modest increase in PSPH compared with L-serine in $SR^{-/-}$ NSCs and a decrease in WT. The magnitude of decrease was greater in WT NSCs, while the increased expression in $SR^{-/-}$ NSCs was smaller compared with untreated controls (Figure 7C). These data suggest that L- and D-serine regulate expression of PSPH via a feedback mechanism (Fell and Snell, 1988; Snell and Fell, 1990). Our data on NSCs from $SR^{-/-}$ showed differences in GFAP expression during differentiation (Figure S1C), suggesting that defects in adult neurogenesis in $SR^{-/-}$ mice may result from defects in astrocytic differentiation (Doetsch, 2003). To determine mature astrocytic differentiation, expression of GFAP was examined. Results show decreased expression of GFAP in differentiating $SR^{-/-}$ NSCs under control conditions (Figure 7A). Treatment with equimolar racemic mixture of L- and D-serine (100 μM) showed increased GFAP expression in $SR^{-/-}$ and modest increase in WT NSCs (Figures 7B and S7C). Similar rescue of NCAM expression (Figure S4B) was observed in WT and $SR^{-/-}$ NSCs treated with L- and D-serine (Figure S7D). Rescue of NCAM expression was greater in WT and $SR^{-/-}$ NSCs treated with L-serine than D-serine (Figure S7D). To determine if levels of malonyl-CoA can be rescued with similar treatment, NSCs grown under control conditions showed approximately 2-fold lower levels in nestin-cre+ compared with $SR^{flox/flox}$, while treatment with exogenous L- and D-serine showed 2-fold and higher levels of malonyl-CoA in both $SR^{flox/flox}$ and nestin-cre+ NSCs. The magnitude of increase was greater with L-serine than D-serine (Figure 7D). These data show both L- and D-serine treatment rescue defects in astrocytic, neuronal differentiation and malonyl-CoA levels.

Model of SR mediated metabolic control of adult SVZ neurogenesis

We present a simplified summary elucidating the role of SR in mediating adult SVZ neurogenesis via lipid metabolism (Figure S6G). SR controls the availability of L-serine and D-serine via the neuron-strocyte shuttle (Wolosker et al., 2017; Ehmsen et al., 2013). Availability of L- and D-serine affects the synthesis of lipids by activation of ACC by an

Figure 5. Expression of AMPK-α, phospho-AMPK, phospho-ACC, and fatty acid metabolism enzymes

(A) Expression of AMPK-α in the mice SVZ.
(B) Expression of *p*-ACC and phospho-AMPK in mice SVZ.
(C) Densitometry of AMPK-α blot shown in (A).
(D) Densitometry of *p*-AMPK blot in (B).
(E) Densitometry plot of *p*-ACC blot in (B).
(F) Relative mRNA levels of *Mcd*, *HaCoA*, and *Ech* in the SVZ of mice.
(G) Relative mRNA levels of *Cpt1a*, *Acc1*, *Spot 14*, and *Cl* in SVZ of mice. Error bars represent SD. Data are representative of three independent experiments. RNA was isolated from n = 5–8 mice per genotype in each experiment.
(H) Schematic of SR-mediated phosphorylation of ACC.

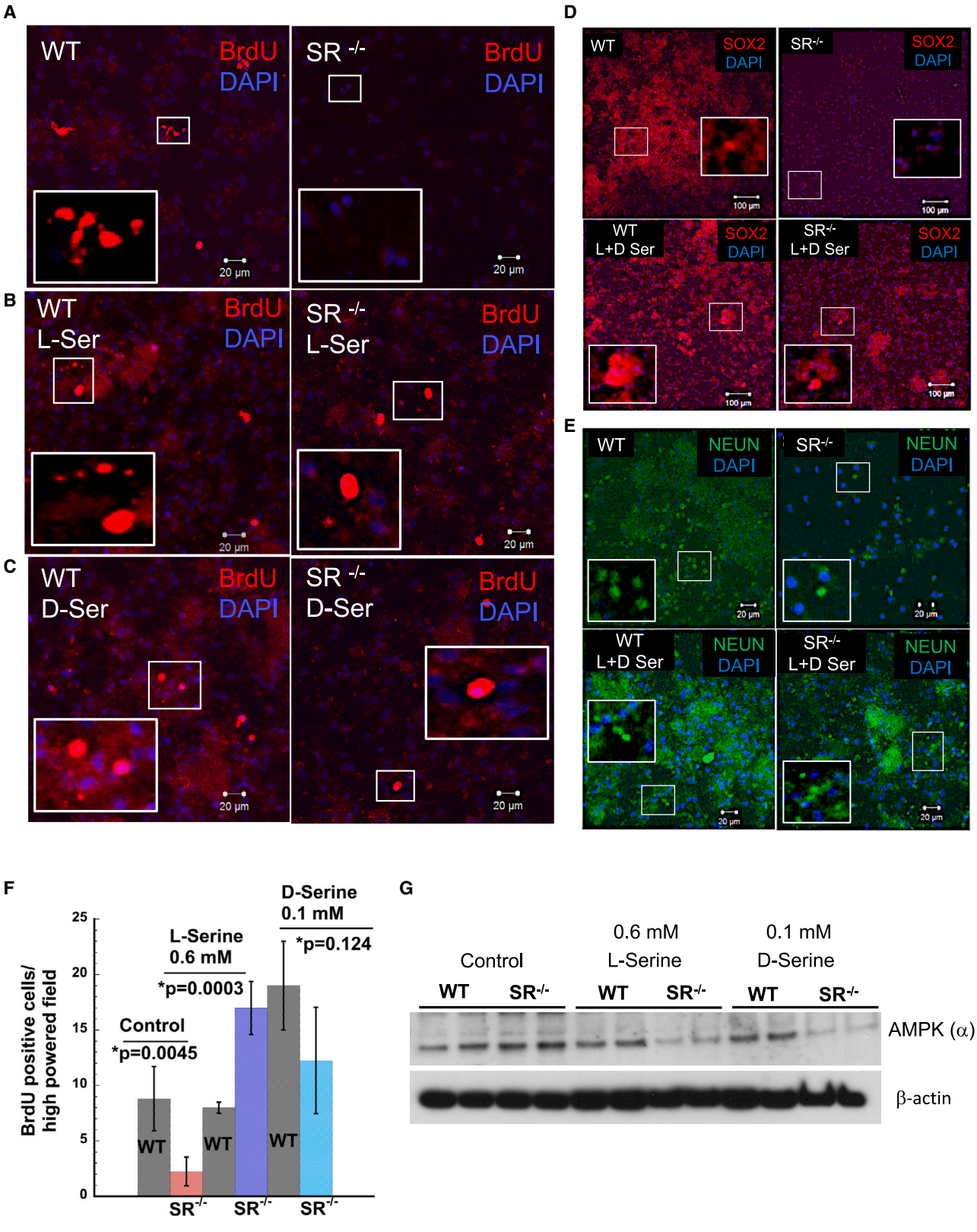

(legend on next page)

unidentified kinase. Overexpression of Spot14 and Mig12 in nestin-cre+ and $SR^{-/-}$ SVZ regulates the catalytic activity of ACC (Knobloch et al., 2013; Park et al., 2013). Activation of ACC by phosphorylation at Ser 79 leads to inhibition of *de novo* fatty acid synthesis by decreasing levels of malonyl-CoA and FASN. Reduction in *de novo* fatty acid synthesis affects the formation of newborn neurons in the SVZ (Type A and B cells) and their proliferation, due to loss of their membrane microenvironment (Clemot et al., 2020; Knobloch et al., 2017).

DISCUSSION

Homeostatic energy changes in the neurogenic niches appear to influence the proliferative properties of adult NSCs. Lipid metabolism plays a major role in adult neurogenesis (Clemot et al., 2020; Knobloch et al., 2013; Knobloch and Jessberger, 2017). D-serine functions as a co-agonist at the NMDA receptor (Balu et al., 2013; Snyder and Kim, 2000). D-serine also mediates adult hippocampal neurogenesis (Sultan et al., 2013) and is involved in proliferation and differentiation of NSCs (Huang et al., 2012). D-cysteine, synthesized by SR plays a role in neurodevelopment (Semenza et al., 2021).

Conditionally deleting *Srr* elicits global changes in lipid profile in the adult SVZ. Our results indicate that SR activates ACC at Ser 79 by an unknown kinase (non-AMPK dependent) and at the tertiary level by affecting polymerization and catalytic activity of ACC due to its interaction with SPOT14 and MIG12 heterocomplex (Knobloch et al., 2013). While L-serine influences cellular proliferation and 1C metabolism, the role of D-serine in mammalian metabolism is unknown.

Lipid rafts are enriched in cholesterol and sphingolipids and involved in stem cell maintenance (Lingwood and Simons, 2010). Our lipidomics data show significant alterations in important lipids in nestin-cre+ SVZ. SR interacts with PSD95 and stargazin in activation of AMPA receptor (Ma et al., 2014). Deletion of *Srr* may impact neuronal metabolism due to serine availability and alteration in membrane signaling pathways. Downregulation of sphingomyelins, ceramides, hexosylceramides, and phosphatidylcholines, a constituent of cell membranes, was seen in nestin-cre+ SVZ. This affects proliferative properties of adult stem cells due to loss of membrane microenvironment.

Deletion of *Srr* downregulated PGDH and PSPH indicating alterations in serine levels. L-serine is a precursor for the synthesis of phosphatidylserine, sphingosine, and ceramide (Esaki et al., 2015). Our lipidomics data reveal 2-fold lower levels of a C_{22} ceramide species Cer22:0_21:0; O3 in nestin-cre+ SVZ. Reduction in C_{16}, C_{18}, C_{20}, C_{22}, and C_{24} acyl chain ceramide species were reported in mouse embryonic fibroblasts under L-serine deprivation (Esaki et al., 2015). Marked reduction in sphingomyelins, ceramides, and hexosylceramides in addition to other lipids was observed under L-serine deprivation in nestin-cre+ SVZ. Deletion of *Srr* results in significant reduction of D-serine synthesis (Balu et al., 2013; Basu et al., 2009). D-serine levels in both neurons and glia are dependent on PGDH, with lower expression leading to decrease in not only L-serine but also D-serine (Ehmsen et al., 2013; Esaki et al., 2015). Altered levels of L- and D-serine may locally affect cellular metabolism and synthesis of lipid precursors like sphingosine affecting the microenvironment of NSCs. Deficits in NSC malonyl-CoA was rescued by L- and D-serine. Rescue experiments showed metabolic compensation, resulting in restored expression of NCAM, SOX2, GFAP, and NEUN respectively.

BrdU incorporation identifies new neurons. $SR^{-/-}$ and nestin-cre+ mice show reduced incorporation of BrdU. Endogenous proliferation marker Ki-67 was also decreased in nestin-cre+ SVZ and in $SR^{-/-}$ primary neurons, highlighting their quiescent nature.

While we observed defects in astrocyte and neuronal differentiation, oligodendrocyte differentiation (OLIG2 expression) was enhanced both in SVZ and in NSCs. Deletion of *Srr* protected against cerebral ischemia and excitotoxicity in mice (Mustafa et al., 2010). Our observations highlight a role for SR in myelination repair with implications for multiple sclerosis and in stroke post recovery (Jia et al., 2019).

Hematopoietic stem cells rely on fatty acid oxidation for maintenance of the stem cell pool (Ito et al., 2012). While D-amino acids comprise peptidoglycans in prokaryotes, their function in mammals is unknown. SR phosphorylates ACC at Ser79, inhibiting synthesis of malonyl-CoA leading to decreased fatty acid synthesis. Interestingly, our data

Figure 6. L- and D-serine rescue defects in SVZ neurogenesis and proliferation *in vitro*

(A) BrdU incorporation in WT and $SR^{-/-}$ NSCs treated with 10 μM BrdU for 18 h at 37°C.

(B) BrdU incorporation in cells treated with 0.6 mM L-serine.

(C) BrdU incorporation in cells treated with 0.1 mM D-serine.

(D) Expression of SOX2 in control (top) and NSCs treated with equimolar mixture of L- and D-serine (100 μM) (lower panel).

(E) Expression of NEUN in differentiating neurons in control (top) and mixture of L- and D-serine (bottom). Scale bar, 100 μm.

(F) Number of BrdU-positive cells per high-powered field in NSCs from WT and $SR^{-/-}$ mice SVZ. An average of 4–5 fields were counted. Error bars represent SD.

(G) Expression of AMPK-α in WT and $SR^{-/-}$ NSCs.

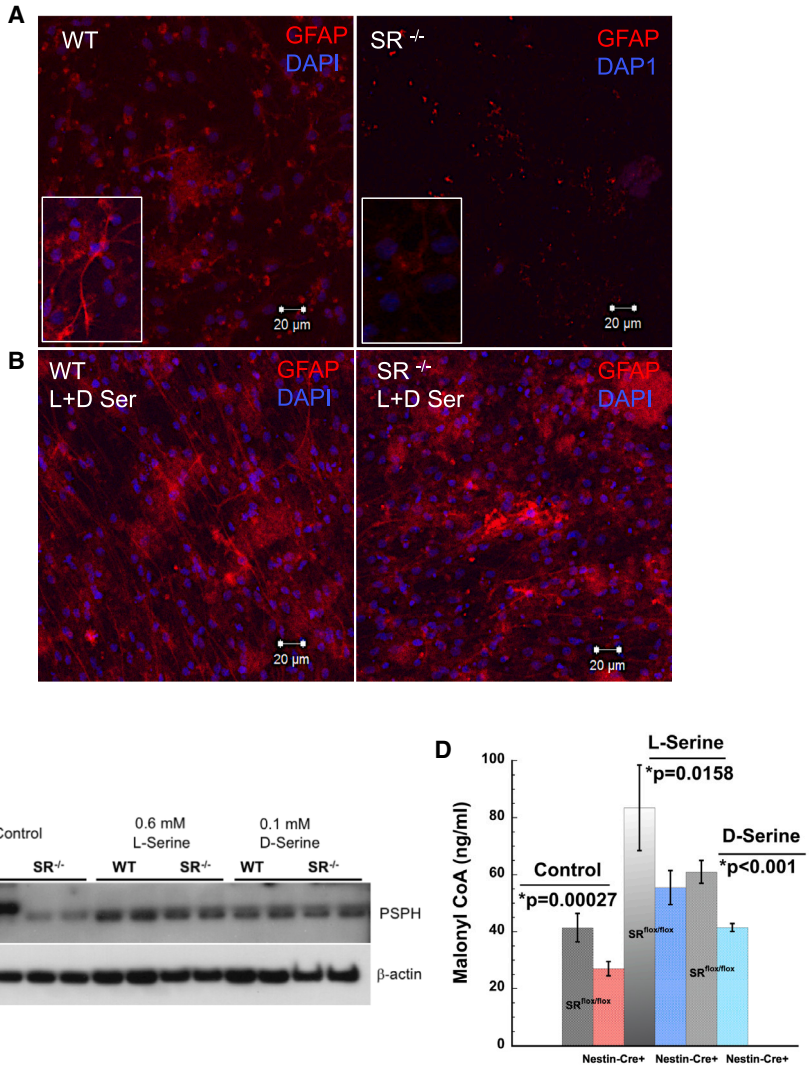

Figure 7. L- and D-serine rescue defects in *de novo* fatty acid synthesis and differentiation

(A) Expression of GFAP (red) in differentiating NSCs from WT and $SR^{-/-}$ mice.

(B) Expression of GFAP in differentiating NSCs from WT and $SR^{-/-}$ mice cultured in the presence of equimolar mixture of L-serine and D-serine (100 μM). Scale bar, 20 μm.

(C) Expression of PSPH in NSCs treated with L-serine and D-serine.

(D) Levels of malonyl-CoA (ng/mL) in NSCs cultured from $SR^{flox/flox}$ and nestin-cre+ mice in the presence of 0.6 mM L-serine and 0.1 mM D-serine. Error bars represent SD. Data are representative of three independent experiments. Tissues for each experiment were pooled from n = 5–8 mice per genotype.

also showed that activation of ACC is independent of AMPK. While nestin-cre+ mice showed increased expression of AMPK dependent on L- and D-serine, it did not undergo activation by phosphorylation at Thr 172, suggesting that SR may activate additional hubs independent of AMPK. We have yet to identify the kinase responsible for ACC activation. Our data show that increased expression of SPOT14 and *Mig12* in nestin-cre+ SVZ may regulate the catalytic activity of ACC due to its effect on ACC polymerization (Knobloch et al., 2013; Park et al., 2013).

Alterations in SVZ fatty acid synthesis affect the NSC microenvironment and their stemness, resulting in reduced newborn neurons and quiescence. We speculate on possible connections between serine and lipid metabolism. Glutamate is a known activator of ACC (Brownsey et al., 2006). Due to structural similarities with glutamate, serine may serve as an activator of ACC. PLP is a structural analog of citrate, which also regulates ACC. PLP inhibits both isoforms of ACC (Brownsey et al., 2006). In the absence of SR, excess unbound PLP may inhibit the activity of ACC, thereby regulating fatty acid synthesis.

In summary, SR plays a role in lipid-mediated adult SVZ neurogenesis via regulation of ACC. Deletion of *Srr* alters levels of L- and D-serine impacting proliferative properties in NSCs. Metabolic control of neurogenesis by supplementation of L- and D-serine may prove beneficial in Alzheimer's disease and schizophrenia that have an underlying component of adult neurogenesis (Le Douce et al., 2020; Schoenfeld and Cameron, 2015; Yun et al., 2016).

EXPERIMENTAL PROCEDURES

See supplemental information for detailed protocols.

Resource availability

Corresponding author

Robin Roychaudhuri (robinroychaudhuri@gmail.com) Current address: University of Maryland School of Medicine, Department. of Obstetrics, Gynecology and Reproductive Sciences, Center for Birth Defects, Baltimore, MD 21201.

Materials availability

All materials will be available upon request to the authors.

Data and code availability

The lipidomics data are available at the National Metabolomics Data Repository (NMDR), the Metabolomics Workbench, https://www.metabolomicsworkbench.org where it has been assigned Study ID ST002705. The data can be accessed directly via its Project DOI: https://doi.org/10.21228/M82H8Q. This work is supported by NIH grant U2C-DK119886 and OT2-OD030544 grant.

Generation of nestin-cre+ SR mice

Nestin-cre+ mice were generated by breeding $SR^{flox/flox}$ mice (Basu et al., 2009) with nestin-cre mice obtained from Jackson labs (number 003771). All animal experiments were approved by the Institutional Animal Care and Use Committee at the Johns Hopkins University School of Medicine.

BrdU (bromodeoxyuridine) labeling

Eight-week-old WT and age-matched $SR^{-/-}$ mice were administered 1 mg/mL BrdU (BromodeoxyUridine) in water by means of a water bottle within the cage for 14 days (*ad libitum*).

Micro dissection of adult mouse brain SVZ

Mice brains were dissected, removed, and kept in sterile PBS. The Petri dish was placed under a dissecting microscope with light source at low magnification on the ventral surface and the olfactory bulbs were removed by holding the cerebellum. The brain was then rotated onto the dorsal aspect and using a sterile blade a coronal cut was made at the level of the optic chiasm (Walker and Kempermann, 2014).

Adherent monolayer stem cell culture

The NSC adherent monolayer culture system is a valuable tool for determining the proliferative and differentiative potential of adult neural stem cells *in vitro*. Cell culture and differentiation of precursor cells in adherent monolayer cultures was followed as per the protocol of Walker and Kempermann (2014).

Neuroblast assay

Neuroblasts (Type A cells) were visualized after plating the cells obtained from dissociation of adherent monolayer cultures following accutase treatment. The dissociated monolayer cells were plated in a 15-μm 24-well plate at 2–3 × 10^5 cells/mL in complete NSC medium supplemented with 20 ng/mL EGF and 10 ng/mL b-FGF.

Mouse FASN ELISA

Mouse FASN (fatty acid synthase) expression in mice brain and SVZ was measured quantitatively using a mouse FASN ELISA kit.

Mouse malonyl-CoA ELISA

Estimation of mouse malonyl-CoA in SVZ lysates was measured quantitatively using a mouse malonyl-CoA ELISA kit.

Quantitative lipidomic analysis

Quantitative lipidomic analysis on SVZ tissue from $SR^{flox/flox}$ and nestin-cre+ mice was performed at The Metabolomics Innovation Center University of Alberta, Canada.

Analysis of gene expression

RNA was isolated from SVZ of WT and $SR^{-/-}$, $SR^{flox/flox}$, and nestin-cre+ mice using an RNA isolation kit. Gene expression studies were performed using the SYBR green method.

Rescue in monolayer adherent cultures

Rescue experiments in adherent monolayer cultures were performed by isolating NSCs from the SVZ of age-matched adult mice. The cells were grown in culture for 7–10 days, following which differentiation was induced by gradual removal of growth factors as mentioned in Walker and Kempermann (2014).

Time spent sniffing novel odor

Mouse olfactory behavior was tested in age-matched WT and $SR^{-/-}$ mice. Mice (n = 20–25 per group) were collected and brought to the behavior suite and the mice were placed in clean cages with new bedding.

Blood glucose estimation

Blood glucose level was monitored by tail bleed using Contour glucometer and Contour blood glucose test strips. Blood glucose measurements were obtained from tail veins at indicated time points post injection.

Insulin ELISA

Quantitative estimation of insulin from brain homogenates and SVZ of age-matched WT, $SR^{-/-}$, $SR^{flox/flox}$, and nestin-cre+ mice was performed using the Ultra Sensitive Mouse Insulin ELISA Kit.

Statistics

Statistical tests were computed using KaleidaGraph (Synergy Software, Reading, PA). Data are represented as mean ± SD. Unpaired Student's t test was used for pairwise comparison with a fixed control condition. For multiple pairwise comparisons with different control and treatment conditions, one-way ANOVA analysis followed by Tukey's post hoc test was used. Values with $p < 0.05$ were considered significant.

SUPPLEMENTAL INFORMATION

Supplemental information can be found online at https://doi.org/10.1016/j.stemcr.2023.05.015.

AUTHOR CONTRIBUTIONS

R.R. conceived, designed, and performed all experiments and analyzed all the data. R.R. wrote, edited, and revised the

manuscript. H.A. performed stem cell differentiation experiments. All authors reviewed the manuscript.

ACKNOWLEDGMENTS

The authors acknowledge Barbara Smith at The Johns Hopkins Microscopy Core Facility for confocal imaging, Lauren Albacarys for performing olfactory behavior tests, Dr. Paul Kim for initial technical assistance, and Evan R. Semenza for helpful discussions. The authors acknowledge Prof. Peixin Yang at the University of Maryland School of Medicine, Department of Obstetrics, Gynecology and Reproductive Sciences for contributing reagents during revision. The work was funded by grant P50 DA044123 from NIDA to S.H.S.

CONFLICT OF INTERESTS

The authors declare no competing interests.

Received: February 1, 2022
Revised: May 21, 2023
Accepted: May 22, 2023
Published: June 22, 2023

REFERENCES

Azari, H., and Reynolds, B.A. (2016). In vitro models for neurogenesis. Cold Spring Harbor Perspect. Biol. *8*.

Azari, H., Sharififar, S., Fortin, J.M., and Reynolds, B.A. (2012). The neuroblast assay: an assay for the generation and enrichment of neuronal progenitor cells from differentiating neural stem cell progeny using flow cytometry. J. Vis. Exp.

Balu, D.T., Li, Y., Puhl, M.D., Benneyworth, M.A., Basu, A.C., Takagi, S., Bolshakov, V.Y., and Coyle, J.T. (2013). Multiple risk pathways for schizophrenia converge in serine racemase knockout mice, a mouse model of NMDA receptor hypofunction. Proc. Natl. Acad. Sci. USA *110*, E2400–E2409.

Basu, A.C., Tsai, G.E., Ma, C.L., Ehmsen, J.T., Mustafa, A.K., Han, L., Jiang, Z.I., Benneyworth, M.A., Froimowitz, M.P., Lange, N., et al. (2009). Targeted disruption of serine racemase affects glutamatergic neurotransmission and behavior. Mol. Psychiatr. *14*, 719–727.

Belvindrah, R., Rougon, G., and Chazal, G. (2002). Increased neurogenesis in adult mCD24-deficient mice. J. Neurosci. *22*, 3594–3607.

Bernal, A., and Arranz, L. (2018). Nestin-expressing progenitor cells: function, identity and therapeutic implications. Cell. Mol. Life Sci. *75*, 2177–2195.

Brownsey, R.W., Boone, A.N., Elliott, J.E., Kulpa, J.E., and Lee, W.M. (2006). Regulation of acetyl-CoA carboxylase. Biochem. Soc. Trans. *34*, 223–227.

Clémot, M., Sênos Demarco, R., and Jones, D.L. (2020). Lipid mediated regulation of adult stem cell behavior. Front. Cell Dev. Biol. *8*, 115.

Declercq, J., Brouwers, B., Pruniau, V.P.E., Stijnen, P., de Faudeur, G., Tuand, K., Meulemans, S., Serneels, L., Schraenen, A., Schuit, F., and Creemers, J.W.M. (2015). Metabolic and behavioural phenotypes in nestin-cre mice are caused by hypothalamic expression of human growth hormone. PLoS One *10*, e0135502.

Doetsch, F. (2003). The glial identity of neural stem cells. Nat. Neurosci. *6*, 1127–1134.

Doetsch, F., Caillé, I., Lim, D.A., García-Verdugo, J.M., and Alvarez-Buylla, A. (1999). Subventricular zone astrocytes are neural stem cells in the adult mammalian brain. Cell *97*, 703–716.

Ehmsen, J.T., Ma, T.M., Sason, H., Rosenberg, D., Ogo, T., Furuya, S., Snyder, S.H., and Wolosker, H. (2013). D-serine in glia and neurons derives from 3-phosphoglycerate dehydrogenase. J. Neurosci. *33*, 12464–12469.

Esaki, K., Sayano, T., Sonoda, C., Akagi, T., Suzuki, T., Ogawa, T., Okamoto, M., Yoshikawa, T., Hirabayashi, Y., and Furuya, S. (2015). L-serine deficiency elicits intracellular accumulation of cytotoxic deoxysphingolipids and lipid body formation. J. Biol. Chem. *290*, 14595–14609.

Faigle, R., and Song, H. (2013). Signaling mechanisms regulating adult neural stem cells and neurogenesis. Biochim. Biophys. Acta *1830*, 2435–2448.

Fell, D.A., and Snell, K. (1988). Control analysis of mammalian serine biosynthesis. Feedback inhibition on the final step. Biochem. J. *256*, 97–101.

Furuya, S., Tabata, T., Mitoma, J., Yamada, K., Yamasaki, M., Makino, A., Yamamoto, T., Watanabe, M., Kano, M., and Hirabayashi, Y. (2000). L-serine and glycine serve as major astroglia-derived trophic factors for cerebellar Purkinje neurons. Proc. Natl. Acad. Sci. USA *97*, 11528–11533.

Gao, X., Lee, K., Reid, M.A., Sanderson, S.M., Qiu, C., Li, S., Liu, J., and Locasale, J.W. (2018). Serine availability influences mitochondrial dynamics and function through lipid metabolism. Cell Rep. *22*, 3507–3520.

Garcia, D., and Shaw, R.J. (2017). AMPK: mechanisms of cellular energy sensing and restoration of metabolic balance. Mol. Cell *66*, 789–800.

González, A., Hall, M.N., Lin, S.C., and Hardie, D.G. (2020). AMPK and TOR: the yin and yang of cellular nutrient sensing and growth control. Cell Metabol. *31*, 472–492.

Harno, E., Cottrell, E.C., and White, A. (2013). Metabolic pitfalls of CNS Cre-based technology. Cell Metabol. *18*, 21–28.

Huang, X., Kong, H., Tang, M., Lu, M., Ding, J.H., and Hu, G. (2012). D-Serine regulates proliferation and neuronal differentiation of neural stem cells from postnatal mouse forebrain. CNS Neurosci. Ther. *18*, 4–13.

Ito, K., Carracedo, A., Weiss, D., Arai, F., Ala, U., Avigan, D.E., Schafer, Z.T., Evans, R.M., Suda, T., Lee, C.H., and Pandolfi, P.P. (2012). A PML-PPAR-delta pathway for fatty acid oxidation regulates hematopoietic stem cell maintenance. Nat. Med. *18*, 1350–1358.

Jia, W., Kamen, Y., Pivonkova, H., and Káradóttir, R.T. (2019). Neuronal activity-dependent myelin repair after stroke. Neurosci. Lett. *703*, 139–144.

Kalhan, S.C., and Hanson, R.W. (2012). Resurgence of serine: an often neglected but indispensable amino Acid. J. Biol. Chem. *287*, 19786–19791.

Kee, N., Sivalingam, S., Boonstra, R., and Wojtowicz, J.M. (2002). The utility of Ki-67 and BrdU as proliferative markers of adult neurogenesis. J. Neurosci. Methods *115*, 97–105.

Kempermann, G. (2006). Adult Neurogenesis Stem Cells and Neuronal Development in the Adult Brain (Oxford University Press).

Knobloch, M. (2017). The role of lipid metabolism for neural stem cell regulation. Brain Plast. *3*, 61–71.

Knobloch, M., Braun, S.M.G., Zurkirchen, L., von Schoultz, C., Zamboni, N., Araúzo-Bravo, M.J., Kovacs, W.J., Karalay, O., Suter, U., Machado, R.A.C., et al. (2013). Metabolic control of adult neural stem cell activity by Fasn-dependent lipogenesis. Nature *493*, 226–230.

Knobloch, M., and Jessberger, S. (2017). Metabolism and neurogenesis. Curr. Opin. Neurobiol. *42*, 45–52.

Knobloch, M., Pilz, G.A., Ghesquière, B., Kovacs, W.J., Wegleiter, T., Moore, D.L., Hruzova, M., Zamboni, N., Carmeliet, P., and Jessberger, S. (2017). A fatty acid oxidation-dependent metabolic shift regulates adult neural stem cell activity. Cell Rep. *20*, 2144–2155.

Knobloch, M., von Schoultz, C., Zurkirchen, L., Braun, S.M.G., Vidmar, M., and Jessberger, S. (2014). SPOT14-positive neural stem/progenitor cells in the hippocampus respond dynamically to neurogenic regulators. Stem Cell Rep. *3*, 735–742.

Le Douce, J., Maugard, M., Veran, J., Matos, M., Jégo, P., Vigneron, P.A., Faivre, E., Toussay, X., Vandenberghe, M., Balbastre, Y., et al. (2020). Impairment of glycolysis-derived l-serine production in astrocytes contributes to cognitive deficits in alzheimer's disease. Cell Metabol. *31*, 503–517.e8.

Lim, D.A., and Alvarez-Buylla, A. (2016). The adult ventricular-subventricular zone (V-SVZ) and olfactory bulb (OB) neurogenesis. Cold Spring Harbor Perspect. Biol. *8*, a018820.

Lingwood, D., and Simons, K. (2010). Lipid rafts as a membrane-organizing principle. Science *327*, 46–50.

Lodhi, I.J., Wei, X., and Semenkovich, C.F. (2011). Lipoexpediency: de novo lipogenesis as a metabolic signal transmitter. Trends Endocrinol. Metabol. *22*, 1–8.

Ma, T.M., Paul, B.D., Fu, C., Hu, S., Zhu, H., Blackshaw, S., Wolosker, H., and Snyder, S.H. (2014). Serine racemase regulated by binding to stargazin and PSD-95: potential N-methyl-D-aspartate-alpha-amino-3-hydroxy-5-methyl-4-isoxazolepropionic acid (NMDA-AMPA) glutamate neurotransmission cross-talk. J. Biol. Chem. *289*, 29631–29641.

Ming, G.L., and Song, H. (2011). Adult neurogenesis in the mammalian brain: significant answers and significant questions. Neuron *70*, 687–702.

Mitoma, J., Furuya, S., and Hirabayashi, Y. (1998). A novel metabolic communication between neurons and astrocytes: non-essential amino acid L-serine released from astrocytes is essential for developing hippocampal neurons. Neurosci. Res. *30*, 195–199.

Moreno-Jiménez, E.P., Flor-García, M., Terreros-Roncal, J., Rábano, A., Cafini, F., Pallas-Bazarra, N., Ávila, J., and Llorens-Martín, M. (2019). Adult hippocampal neurogenesis is abundant in neurologically healthy subjects and drops sharply in patients with Alzheimer's disease. Nat. Med. *25*, 554–560.

Mustafa, A.K., Ahmad, A.S., Zeynalov, E., Gazi, S.K., Sikka, G., Ehmsen, J.T., Barrow, R.K., Coyle, J.T., Snyder, S.H., and Doré, S. (2010). Serine racemase deletion protects against cerebral ischemia and excitotoxicity. J. Neurosci. *30*, 1413–1416.

Park, S., Hwang, I.W., Makishima, Y., Perales-Clemente, E., Kato, T., Niederländer, N.J., Park, E.Y., and Terzic, A. (2013). Spot14/Mig12 heterocomplex sequesters polymerization and restrains catalytic function of human acetyl-CoA carboxylase 2. J. Mol. Recogn. *26*, 679–688.

Pevny, L.H., and Nicolis, S.K. (2010). Sox2 roles in neural stem cells. Int. J. Biochem. Cell Biol. *42*, 421–424.

Reid, M.A., Allen, A.E., Liu, S., Liberti, M.V., Liu, P., Liu, X., Dai, Z., Gao, X., Wang, Q., Liu, Y., et al. (2018). Serine synthesis through PHGDH coordinates nucleotide levels by maintaining central carbon metabolism. Nat. Commun. *9*, 5442.

Schell, M.J., Brady, R.O., Jr., Molliver, M.E., and Snyder, S.H. (1997). D-serine as a neuromodulator: regional and developmental localizations in rat brain glia resemble NMDA receptors. J. Neurosci. *17*, 1604–1615.

Schoenfeld, T.J., and Cameron, H.A. (2015). Adult neurogenesis and mental illness. Neuropsychopharmacology *40*, 113–128.

Semenza, E.R., Harraz, M.M., Abramson, E., Malla, A.P., Vasavda, C., Gadalla, M.M., Kornberg, M.D., Snyder, S.H., and Roychaudhuri, R. (2021). D-cysteine is an endogenous regulator of neural progenitor cell dynamics in the mammalian brain. Proc. Natl. Acad. Sci. USA *118*. e2110610118.

Snell, K., and Fell, D.A. (1990). Metabolic control analysis of mammalian serine metabolism. Adv. Enzym. Regul. *30*, 13–32.

Snyder, S.H., and Kim, P.M. (2000). D-amino acids as putative neurotransmitters: focus on D-serine. Neurochem. Res. *25*, 553–560.

Steinberg, G.R., Macaulay, S.L., Febbraio, M.A., and Kemp, B.E. (2006). AMP-activated protein kinase–the fat controller of the energy railroad. Can. J. Physiol. Pharmacol. *84*, 655–665.

Sultan, S., Gebara, E.G., Moullec, K., and Toni, N. (2013). D-serine increases adult hippocampal neurogenesis. Front. Neurosci. *7*, 155.

Tong, C.K., and Alvarez-Buylla, A. (2014). SnapShot: adult neurogenesis in the V-SVZ. Neuron *81*, 220–220.e1.

Walker, T.L., and Kempermann, G. (2014). One mouse, two cultures: isolation and culture of adult neural stem cells from the two neurogenic zones of individual mice. J. Vis. Exp., e51225.

Wang, Y.Z., Fan, H., Ji, Y., Reynolds, K., Gu, R., Gan, Q., Yamagami, T., Zhao, T., Hamad, S., Bizen, N., et al. (2020). Olig2 regulates terminal differentiation and maturation of peripheral olfactory sensory neurons. Cell. Mol. Life Sci. *77*, 3597–3609.

Wiese, C., Rolletschek, A., Kania, G., Blyszczuk, P., Tarasov, K.V., Tarasova, Y., Wersto, R.P., Boheler, K.R., and Wobus, A.M. (2004). Nestin expression–a property of multi-lineage progenitor cells? Cell. Mol. Life Sci. *61*, 2510–2522.

Witt, R.M., Galligan, M.M., Despinoy, J.R., and Segal, R. (2009). Olfactory behavioral testing in the adult mouse. J. Vis. Exp., 949.

Wolosker, H., Balu, D.T., and Coyle, J.T. (2017). Astroglial versus neuronal D-serine: check your controls. Trends Neurosci. *40*, 520–522.

Wolosker, H., Blackshaw, S., and Snyder, S.H. (1999a). Serine racemase: a glial enzyme synthesizing D-serine to regulate glutamate-N-methyl-D-aspartate neurotransmission. Proc. Natl. Acad. Sci. USA *96*, 13409–13414.

Wolosker, H., Sheth, K.N., Takahashi, M., Mothet, J.P., Brady, R.O., Jr., Ferris, C.D., and Snyder, S.H. (1999b). Purification of serine racemase: biosynthesis of the neuromodulator D-serine. Proc. Natl. Acad. Sci. USA *96*, 721–725.

Yamasaki, M., Yamada, K., Furuya, S., Mitoma, J., Hirabayashi, Y., and Watanabe, M. (2001). 3-Phosphoglycerate dehydrogenase, a key enzyme for l-serine biosynthesis, is preferentially expressed in the radial glia/astrocyte lineage and olfactory ensheathing glia in the mouse brain. J. Neurosci. *21*, 7691–7704.

Yun, S., Reynolds, R.P., Masiulis, I., and Eisch, A.J. (2016). Re-evaluating the link between neuropsychiatric disorders and dysregulated adult neurogenesis. Nat. Med. *22*, 1239–1247.

Stem Cell Reports, Volume *18*

Supplemental Information

Serine Racemase mediates subventricular zone neurogenesis via fatty acid metabolism

Robin Roychaudhuri, Hasti Atashi, and Solomon H. Snyder

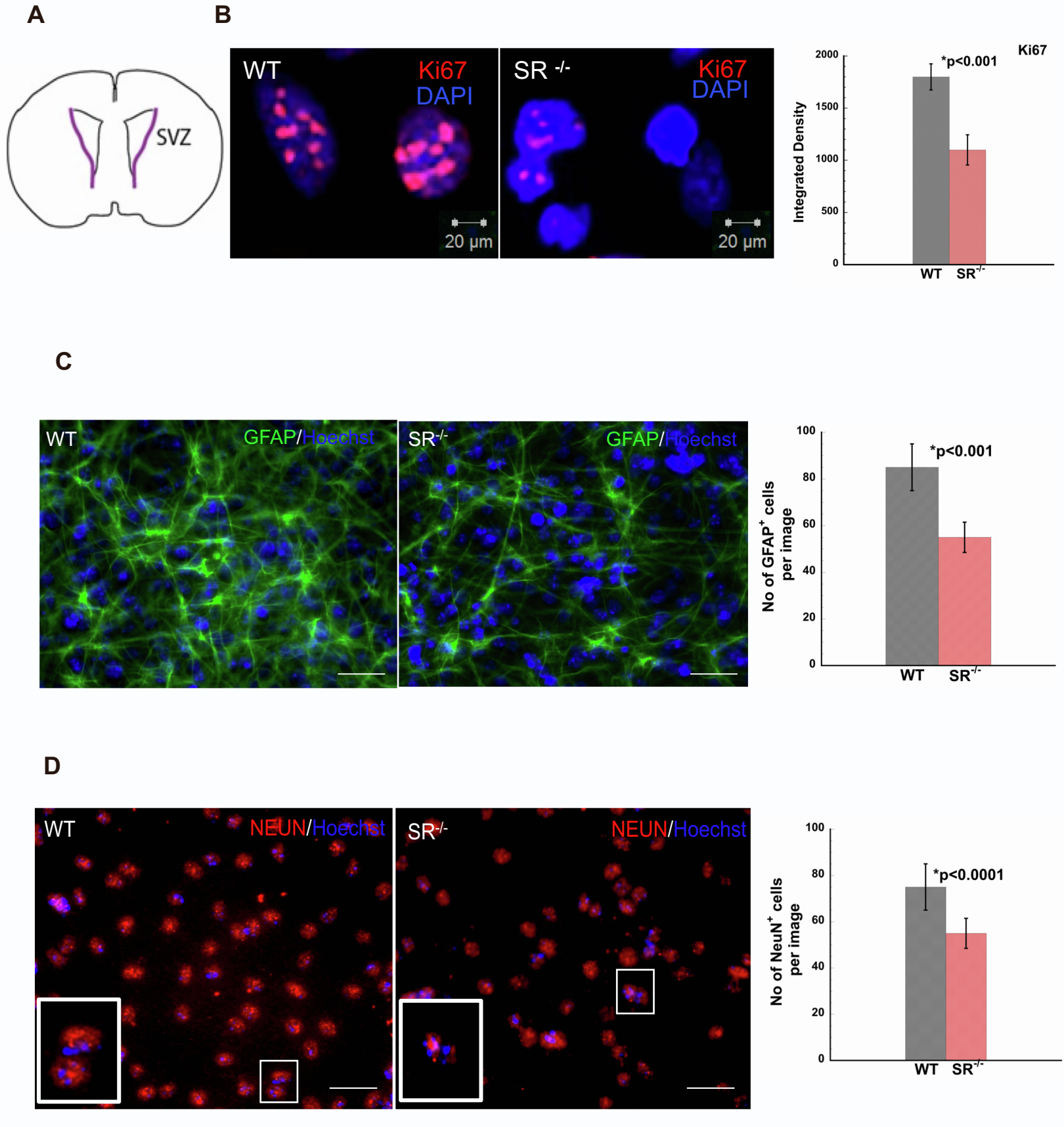
A
B
SVZ
WT
Ki67
DAPI
20 µm
SR -/-
Ki67
DAPI
20 µm
Ki67
*p<0.001
Integrated Density
2000
1500
1000
500
0
WT
SR-/-
C
WT
GFAP/Hoechst
SR-/-
GFAP/Hoechst
*p<0.001
No of GFAP+ cells per image
100
80
60
40
20
0
WT
SR-/-
D
WT
NEUN/Hoechst
SR-/-
NEUN/Hoechst
*p<0.0001
No of NeuN+ cells per image
100
80
60
40
20
0
WT
SR-/-

Suppl Fig 1.

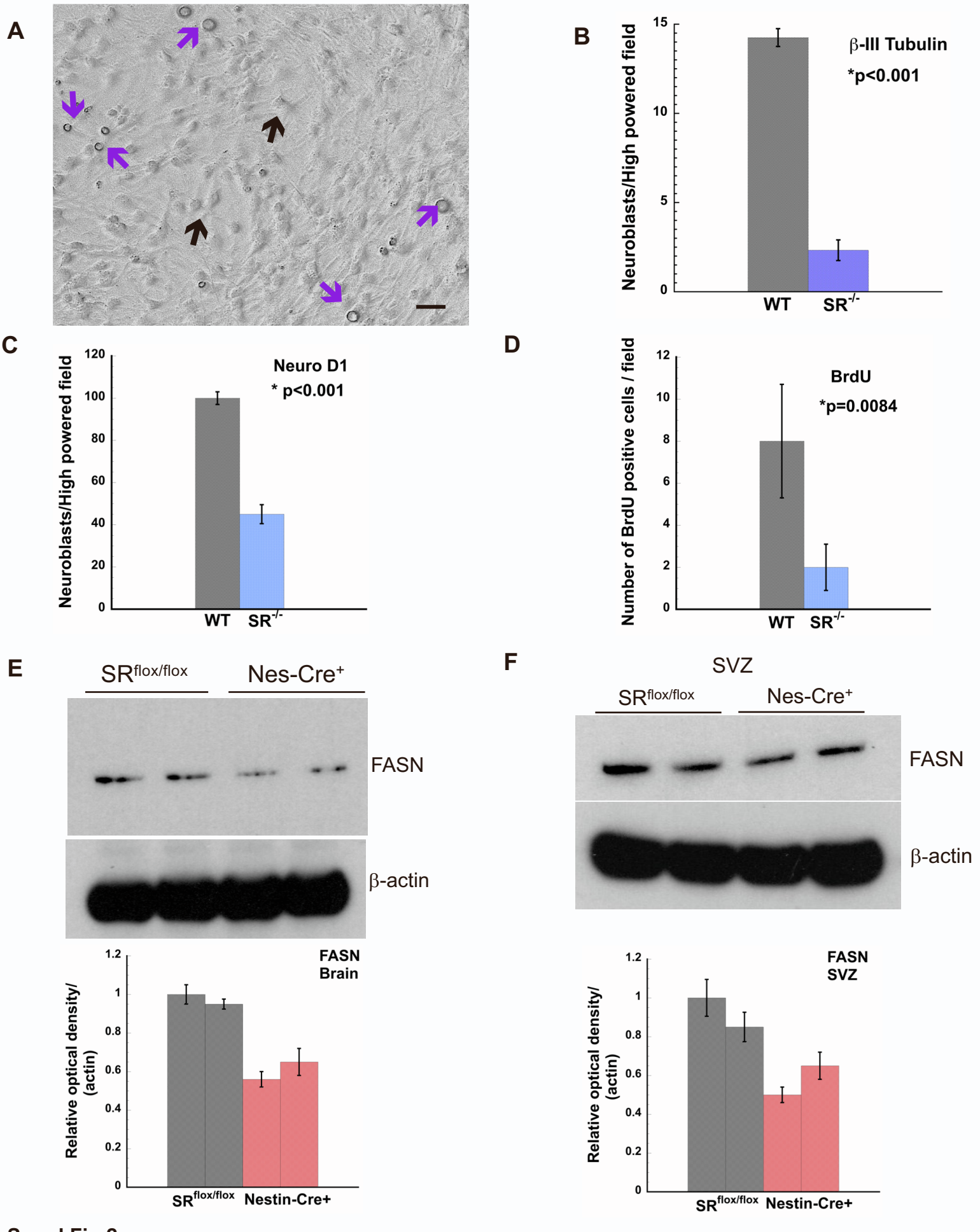
A
B
β-III Tubulin
*p<0.001
Neuroblasts/High powered field
WT
SR-/-
C
Neuro D1
* p<0.001
Neuroblasts/High powered field
WT
SR-/-
D
BrdU
*p=0.0084
Number of BrdU positive cells / field
WT
SR-/-
E
SRflox/flox
Nes-Cre+
FASN
β-actin
FASN
Brain
Relative optical density/ (actin)
SRflox/flox
Nestin-Cre+
F
SVZ
SRflox/flox
Nes-Cre+
FASN
β-actin
FASN
SVZ
Relative optical density/ (actin)
SRflox/flox
Nestin-Cre+

Suppl Fig 2.

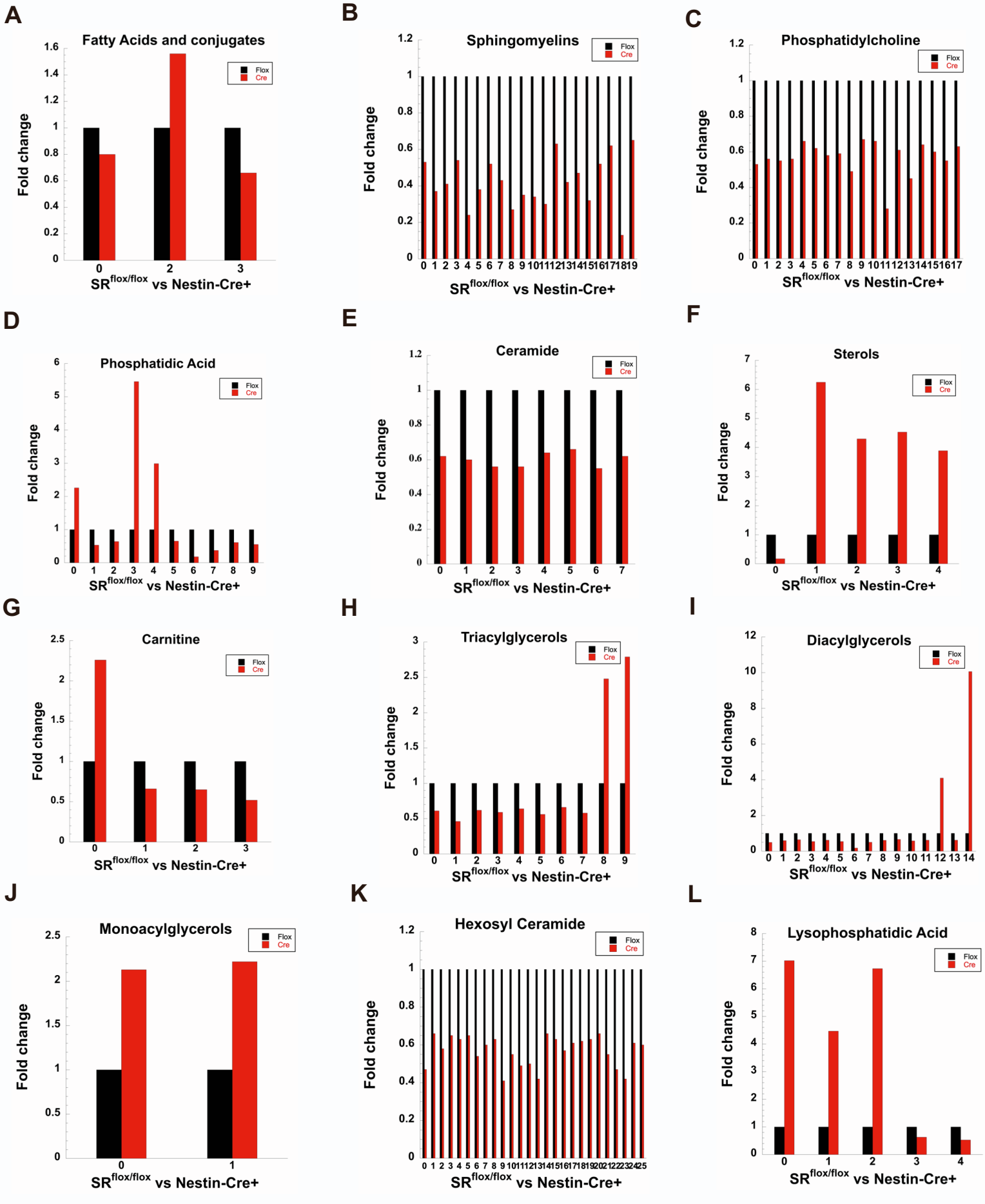
A
Fatty Acids and conjugates
Flox
Cre
Fold change
SR flox/flox vs Nestin-Cre+
B
Sphingomyelins
C
Phosphatidylcholine
D
Phosphatidic Acid
E
Ceramide
F
Sterols
G
Carnitine
H
Triacylglycerols
I
Diacylglycerols
J
Monoacylglycerols
K
Hexosyl Ceramide
L
Lysophosphatidic Acid

Suppl Fig 3.

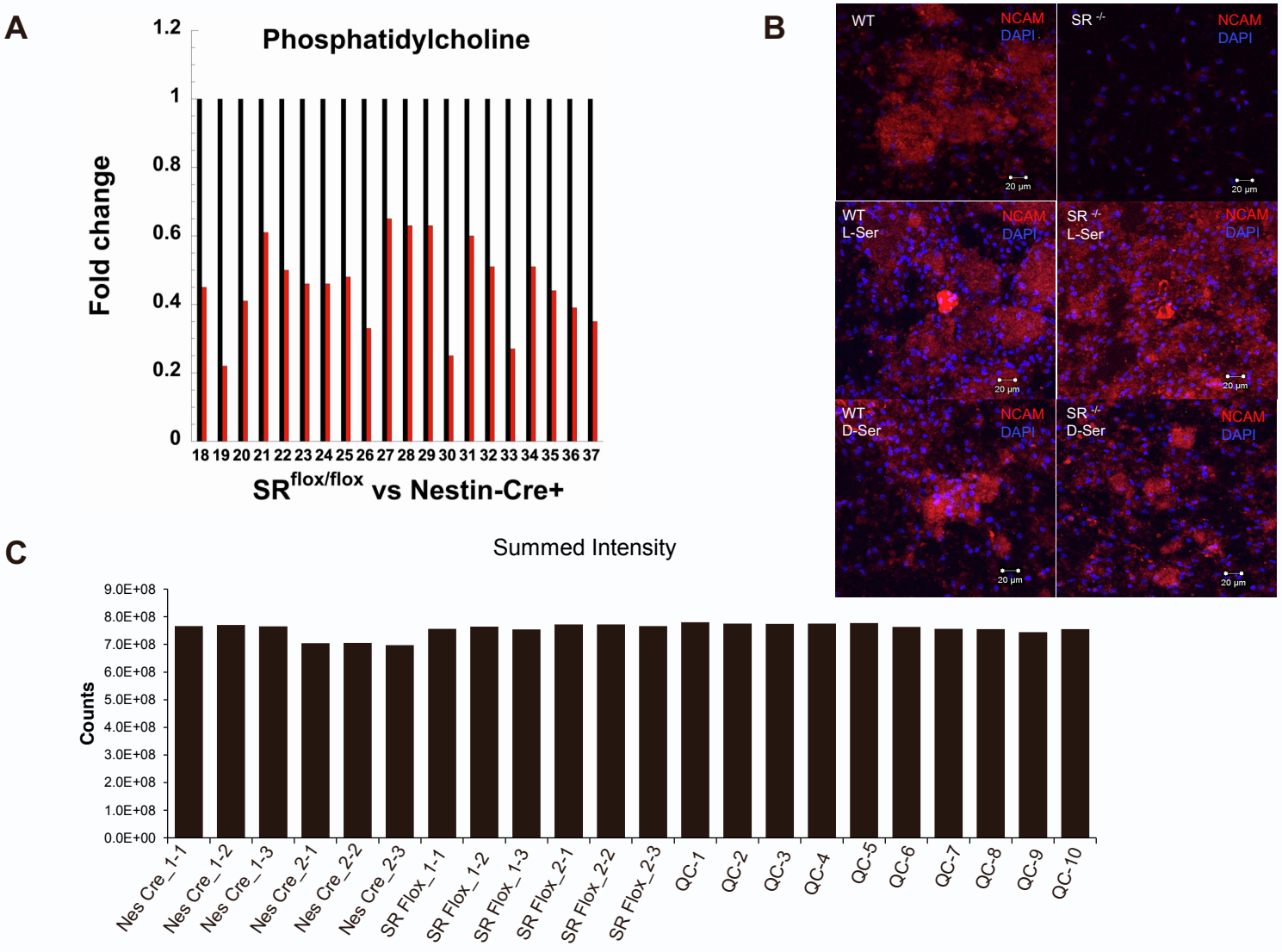
A
Phosphatidylcholine
Fold change
1.2
1
0.8
0.6
0.4
0.2
0
18 19 20 21 22 23 24 25 26 27 28 29 30 31 32 33 34 35 36 37
SR flox/flox vs Nestin-Cre+
B
WT
NCAM
DAPI
SR -/-
WT L-Ser
SR -/- L-Ser
WT D-Ser
SR -/- D-Ser
20 µm
C
Summed Intensity
Counts
9.0E+08
8.0E+08
7.0E+08
6.0E+08
5.0E+08
4.0E+08
3.0E+08
2.0E+08
1.0E+08
0.0E+00
Nes Cre_1-1
Nes Cre_1-2
Nes Cre_1-3
Nes Cre_2-1
Nes Cre_2-2
Nes Cre_2-3
SR Flox_1-1
SR Flox_1-2
SR Flox_1-3
SR Flox_2-1
SR Flox_2-2
SR Flox_2-3
QC-1
QC-2
QC-3
QC-4
QC-5
QC-6
QC-7
QC-8
QC-9
QC-10
D
WT
BrdU
GFAP
20 µm
E
SR Flox
mCD24
DAPI
Nes Cre
20 µm
*p<0.001
No of mCD24+ cells per mm2
15
10
5
0
SR flox/flox Nestin-Cre+

Suppl Fig 4.

A

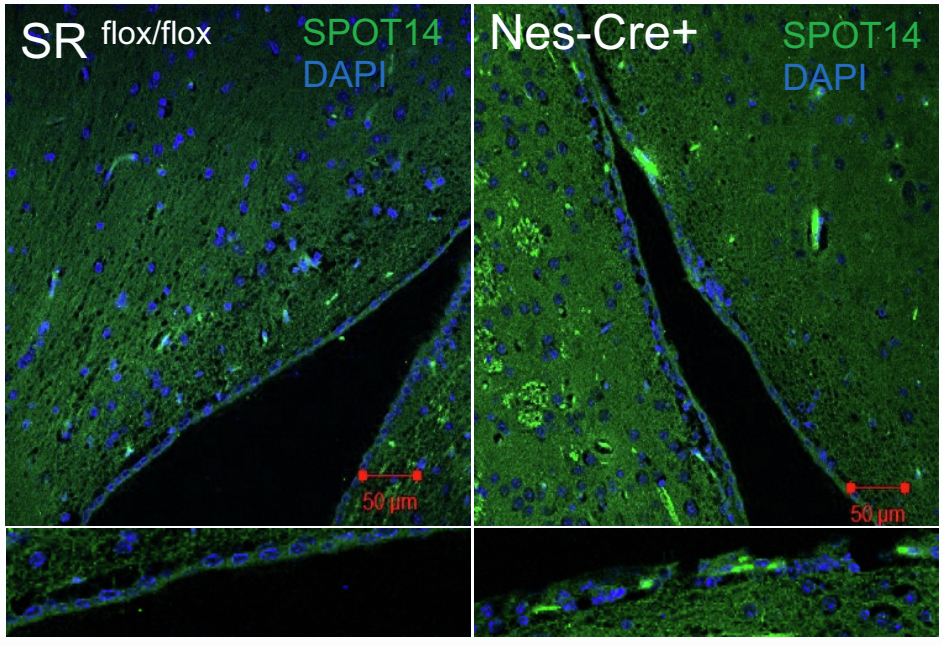

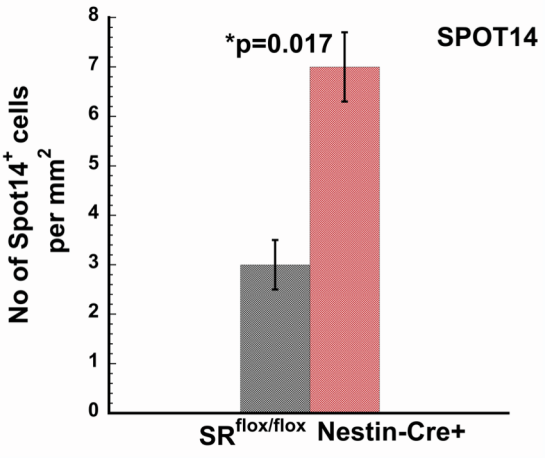

B

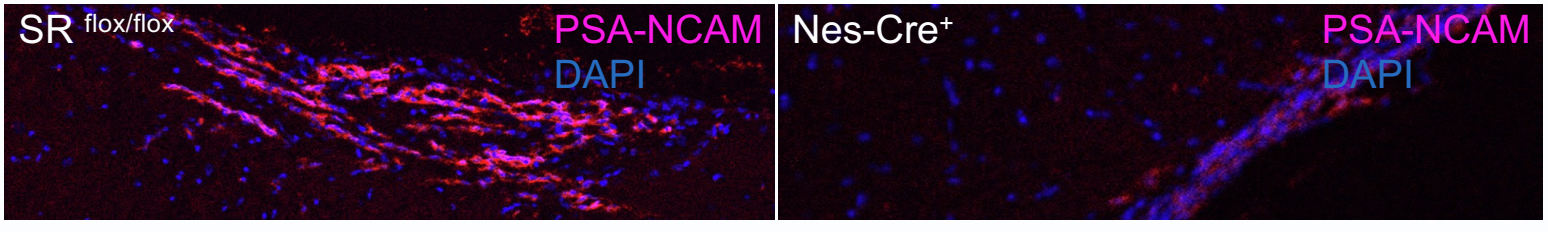

C

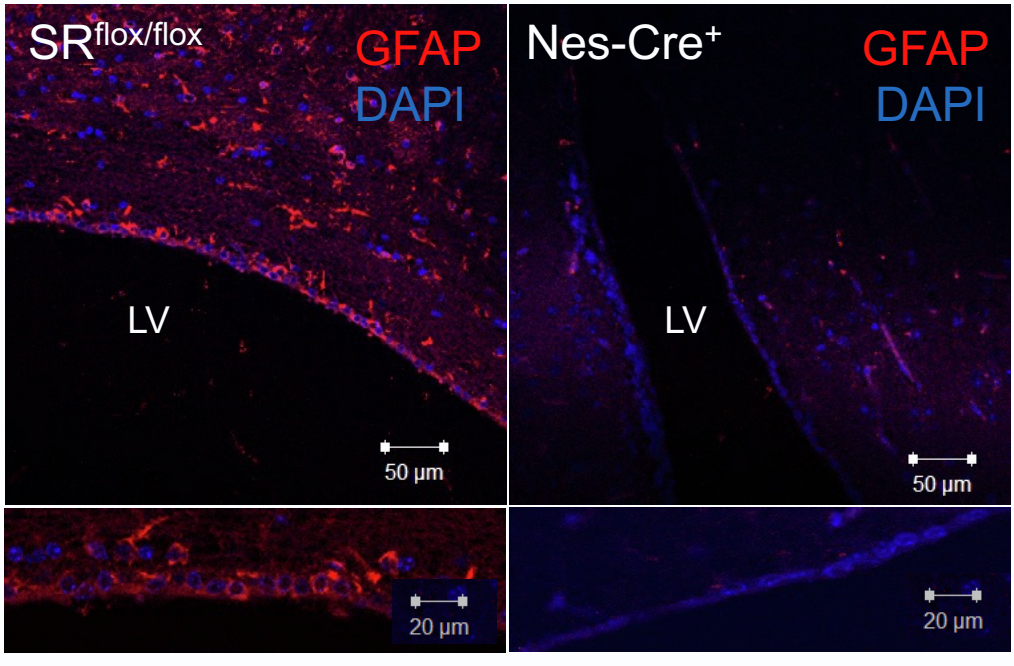

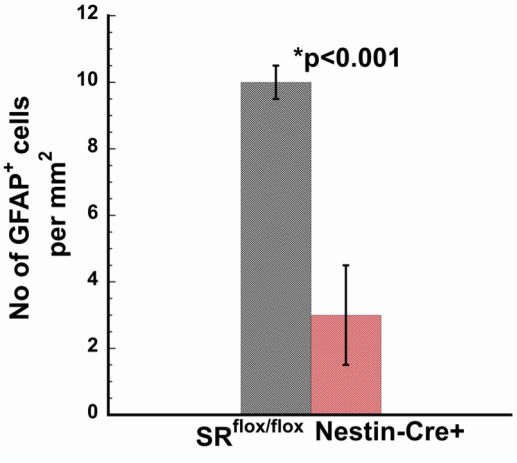

Suppl Fig 5.

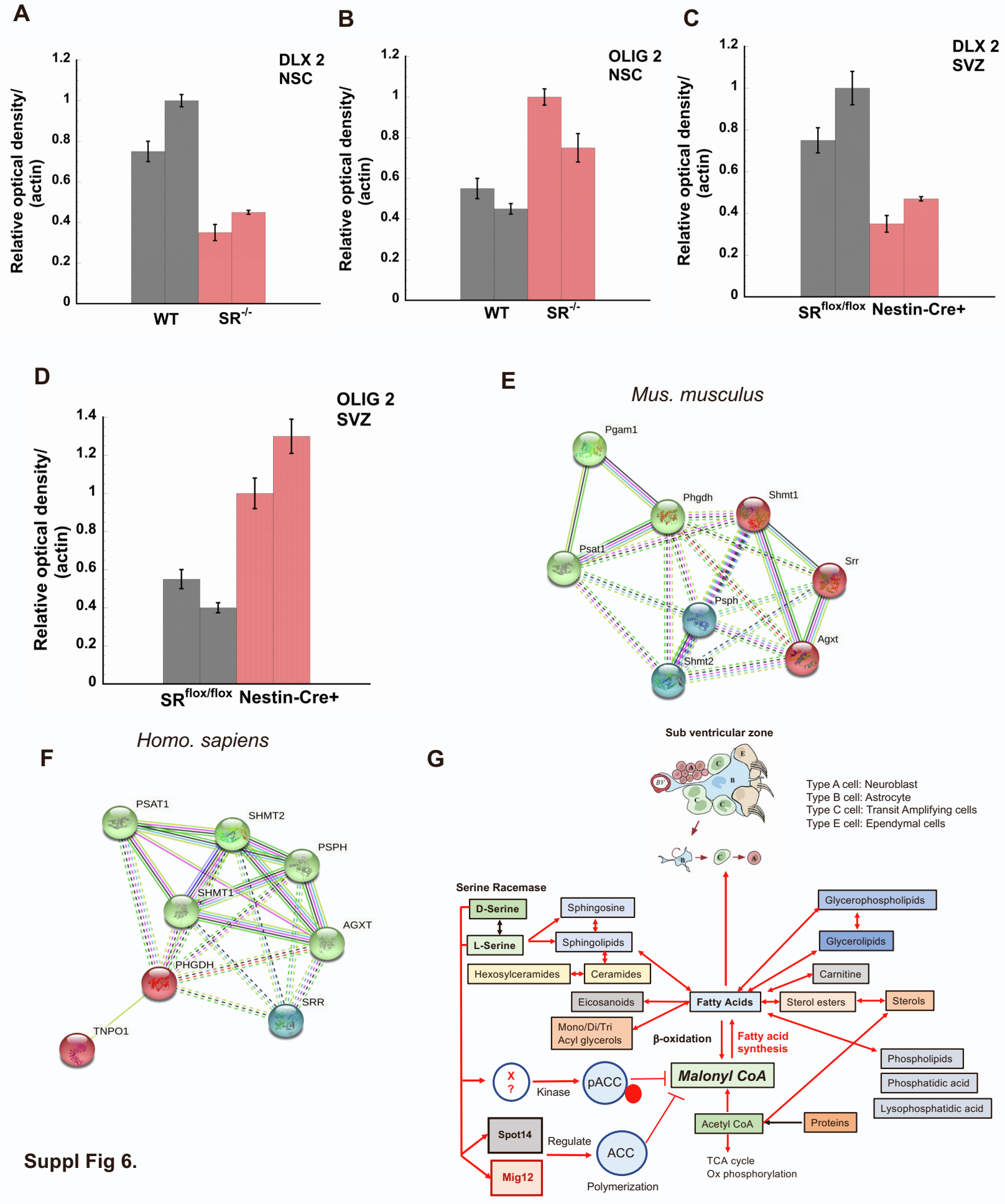
A
DLX 2
NSC
Relative optical density/ (actin)
1.2
1
0.8
0.6
0.4
0.2
0
WT
SR-/-
B
OLIG 2
NSC
Relative optical density/ (actin)
WT
SR-/-
C
DLX 2
SVZ
Relative optical density/ (actin)
SRflox/flox Nestin-Cre+
D
OLIG 2
SVZ
Relative optical density/ (actin)
1.4
1.2
SRflox/flox Nestin-Cre+
E
Mus. musculus
Pgam1
Phgdh
Shmt1
Psat1
Srr
Psph
Agxt
Shmt2
F
Homo. sapiens
PSAT1
SHMT2
PSPH
SHMT1
AGXT
PHGDH
SRR
TNPO1
G
Sub ventricular zone
Type A cell: Neuroblast
Type B cell: Astrocyte
Type C cell: Transit Amplifying cells
Type E cell: Ependymal cells
Serine Racemase
D-Serine
L-Serine
Sphingosine
Sphingolipids
Hexosylceramides
Ceramides
Glycerophospholipids
Glycerolipids
Carnitine
Eicosanoids
Fatty Acids
Sterol esters
Sterols
Mono/Di/Tri Acyl glycerols
β-oxidation
Fatty acid synthesis
Phospholipids
Phosphatidic acid
Lysophosphatidic acid
X ?
Kinase
pACC
Malonyl CoA
Acetyl CoA
Proteins
Spot14
Mig12
Regulate
ACC
Polymerization
TCA cycle
Ox phosphorylation

Suppl Fig 6.

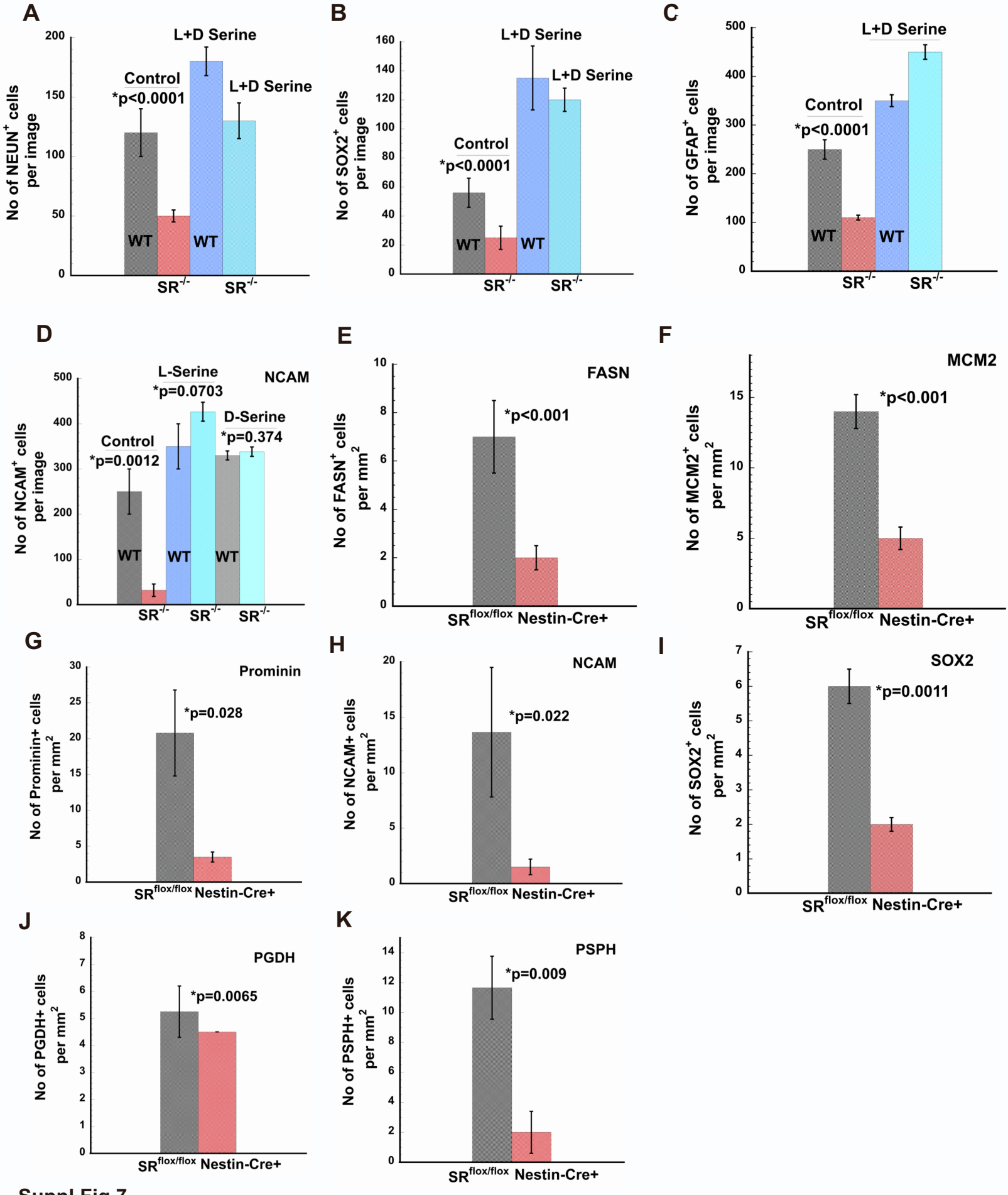
A
No of NEUN+ cells per image
Control
*p<0.0001
L+D Serine
L+D Serine
WT
WT
SR-/-
SR-/-
B
No of SOX2+ cells per image
Control
*p<0.0001
L+D Serine
L+D Serine
C
No of GFAP+ cells per image
Control
*p<0.0001
L+D Serine
D
No of NCAM+ cells per image
L-Serine
*p=0.0703
NCAM
Control
*p=0.0012
D-Serine
*p=0.374
E
No of FASN+ cells per mm2
*p<0.001
FASN
SRflox/flox Nestin-Cre+
F
No of MCM2+ cells per mm2
*p<0.001
MCM2
G
No of Prominin+ cells per mm2
*p=0.028
Prominin
H
No of NCAM+ cells per mm2
*p=0.022
NCAM
I
No of SOX2+ cells per mm2
*p=0.0011
SOX2
J
No of PGDH+ cells per mm2
*p=0.0065
PGDH
K
No of PSPH+ cells per mm2
*p=0.009
PSPH

Suppl Fig 7.

Supplemental Figures and Tables legend.

Suppl Fig 1. (**A**) Schematic of mouse SVZ (**B**) Ki67 staining in WT and $SR^{-/-}$ primary neurons derived from SVZ neural stem cells Scale Bar=20 μm. (**C**) GFAP (**D**) NeuN expression in differentiated WT and $SR^{-/-}$ neural stem cells in culture. DAPI (nuclear stain) is indicated in blue. Scale Bar= 100 μm. Data are representative of 3 independent experiments. Cells were counted in multiple high-powered fields. Error Bars are SD. *Related to Figure 1 and 2.*

Suppl Fig 2. (**A**) Phase contrast image of neuroblasts (purple arrows) on a bed of astrocytes (black arrows) in the neuroblast assay. Neuroblasts appear 3-4 days after induction of differentiation. Scale Bar=20 μm (**B**) Expression of β-III Tubulin, a marker for neuroblasts. *$p<0.001$ relative to WT control. Neuroblasts were counted in each of the different high powered fields in each genotype. (**C**) Expression of NeuroD1, a marker for neuroblasts. *$p<0.001$ relative to WT control. Data are representative of 3 independent experiments. Error Bars are SD. (**D**) BrdU (Bromo deoxy Uridine) incorporation in NSCs from WT and $SR^{-/-}$ mice SVZ after incubation for 18 h with 10 μM BrdU. BrdU positive cells were counted in the different high powered fields. *$p=0.0084$ relative to WT control. Error Bars refer to SD. (**E**) Expression of mouse FASN in whole brain lysates of $SR^{flox/flox}$ and nestin-cre+ mice. (**F**) Expression of mouse FASN in SVZ lysates of $SR^{flox/flox}$ and nestin-cre+ mice. All samples are run in duplicate and tissues pooled from 5-10

mice/experiment. Actin was a loading control. Plot shows densitometry of the blots. *Related to Figures 1 and 2.*

Suppl Fig 3. Plots show fold changes in the expression (Y-axis) of lipids in the different classes that are significantly altered in the SVZ of adult SR $^{flox/flox}$ and nestin-cre+ mice following a global lipidomics screen by UPLC-MS/MS. Numbers on the X-axis in the different plots show the specific lipid molecules in the respective classes that are listed in Table S2. (**A**) Fatty Acid conjugates (**B**) Sphingomyelins (**C**) Phosphatidylcholine (**D**) Phosphatidic Acid (**E**) Ceramides (**F**) Sterols (**G**) Carnitines (**H**) Triacylglycerols (**I**) Diacylglycerols (**J**) Monoacylglycerols (**K**) Hexosyl Ceramides (**L**) Lysophosphatidic Acid. *Related to Figure 4.*

Suppl Fig 4. (**A**) Fold change in expression of phosphatidylcholine in the SVZ of SR $^{flox/flox}$ and nestin-cre+ mice from a global lipidomics screen by LC-MS/MS. Numbers on the x-axis indicate individual molecules within the group. The molecules are listed in Table S4. Y axis indicates fold change in expression relative to SR $^{flox/flox}$ control. (**B**) NCAM expression in WT and SR$^{-/-}$ NSCs grown under control, L and D-serine rescue conditions Scale Bar=20 μm (**C**) Summed intensity for all detected features in each LC-MS/MS sample injection in SR $^{flox/flox}$ and nestin-cre+ SVZ after merging positive and negative ionization modes. QC refers to quality control sample. (**D**) Representative enlarged section of the lateral ventricle of the SVZ of WT mice showing incorporation of BrdU (red) and GFAP (green). (**E**) Enlarged image of the lateral ventricle of SVZ in SR $^{flox/flox}$ and nestin-cre+ mice showing expression of mCD24 (red) in the different high powered fields.

Scale Bar=20 μm. Data are representative of 3 independent experiments with an N=4-8 mice per genotype/experiment. Error Bars are SD. DAPI is seen in blue. *Related to Figures 1, 2 and 4.*

Suppl Fig 5. (**A**) Expression of SPOT14 (green) in SR $^{flox/flox}$ and nestin-cre+ mice SVZ along the lateral ventricle per high powered field. Scale bar=50 μm. (top panel). Lower panel shows an enlarged section. (**B**) Expression of PSA-NCAM (pink) along the rostral migratory stream in SR $^{flox/flox}$ and nestin-cre+ mice. Panel shows an enlarged section. (**C**) Expression of GFAP (red) in the lateral ventricle (LV) of SVZ of adult SR $^{flox/flox}$ and nestin-cre+ mice per high powered field. Data represent 3 independent experiments with N=4-6 mice per genotype per experiment. Lower panel shows an enlarged section of the above figure. Scale bar=50 μm (top panel) and 20 μm (bottom panel). DAPI is indicated in blue. *Related to Figures 1 and 2.*

Suppl Fig 6. Densitometric plots of western blots of (**A**) DLX2 (**B**) OLIG2 from NSC lysates of age matched WT and SR$^{-/-}$ mice. (**C**) DLX2 (**D**) OLIG2 from SVZ tissue lysates of age matched SR $^{flox/flox}$ and nestin-cre+ SVZ. Samples were run in duplicate. In each lysate sample, SVZ tissue was pooled from N=5-10 mice/experiment. *Related to Figures 1 and 2*. (**E**) STRING analysis of SR with PGDH and PSPH in mouse database (**F**) human database. *Related to Figures 3 and 5.* (**G**) Simplified schematic of the different lipid classes that are under control of SR in the SVZ of adult mice based on a global lipidomics screen. SR alters lipid metabolism at the primary level by phosphorylation of ACC at Ser 79 and at the tertiary level by altering polymerization of ACC and its loss of catalytic

activity by SPOT14-MIG12 heterocomplex interaction, leading to decrease in malonyl CoA synthesis and decrease in *de novo* fatty acid synthesis by FASN. SVZ schematic was adapted from (Pircs et al., 2018). pACC (phospho Acetyl CoA Carboxylase), TCA (tricarboxylic acid). Ox phos (oxidative phosphorylation). *Related to Figures 4 and 5, Suppl figs 3 and 4.*

Suppl Fig 7. Plots show quantitative analysis of (**A**) NEUN (**B**) SOX2 (**C**) GFAP (**D**) NCAM positive staining in rescue experiments performed with SVZ NSCs from WT and $SR^{-/-}$ mice. Expression of (**E**) FASN (**F**) MCM2 (**G**) Prominin (**H**) NCAM (**I**) SOX2 (**J**) PGDH (**K**) PSPH in SVZ of age matched $SR^{flox/flox}$ and nestin-cre+ mice. Error Bars refer to SD. * indicates p value between the groups. (student's *t-test* and ANOVA). *Related to Figures 2, 3, 6, and 7*.

Suppl Tables Legend.

Table S1. Table shows the 15 most important lipids identified in the lipidomics screen in the SVZ of age matched adult $SR^{flox/flox}$ and nestin-cre+ mice. Table shows unique identification number, lipid molecule and the class. *Related to Fig. 4F*.

Table S2. Table 2 identities all the lipid molecules from the lipidomics screen in the different lipid classes. Number in each table indicates the lipid molecule identified in the respective class (plotted in suppl fig. 3 on x axis), followed by the lipid ID and fold change in nestin-cre+ mice relative to $SR^{flox/flox}$ (on y-axis). *Related to Fig. 4E*.

Table S3. Table 3 shows the list of primer sequences used for gene expression studies using the SYBR Green method. *Related to Fig. 3B,3I and 5F-G*.

Table S4. Table shows all the lipids identified in the SVZ of SR $^{flox/flox}$ and nestin-cre+ lipidomics heatmap with m/z value, best matched lipid followed by their subclass. *Related to Fig. 4E*.

Table S5. Table shows the abbreviations of the different lipid subclasses identified in the UPLC-MS MS lipidomics screen. *Related to Figure 4 and Suppl figs 3 and 4.*

Supplemental Experimental Procedures:

Reagents: Purified L-serine and D-serine, were purchased from Sigma Chemical Corp. All salts for buffers and reagents were of research grade and high purity. Milli Q water was used to make buffers and solutions for experiments. HPLC grade solvents and water (Fisher Scientific) was used for estimation of D and L-Serine. Antibodies for rabbit Ki67 (Novus Bio; NB500-170SS), rabbit FASN (Bethyl Labs; A301-324A-T), mouse PSA-NCAM (DSHB Iowa; 5A5-c), mouse Spot14 (sc-137178; Santacruz Biotechnology), rabbit MCM2 (Bethyl Labs; IHC-00009-T), mouse BrdU (Sigma; B8434-25 μl), mouse CD24 (eBioscience; #14-0242-82), rabbit Prominin (Millipore; ZRB1013-25 μl) antibodies were purchased from the vendors mentioned in parenthesis next to the antibody. Antibodies for immunocytochemistry were rabbit NEUN (Cell Signaling Technology; D4G40), β III-Tubulin (RND Systems; #MAB1195-SP), mouse GFAP (Millipore; MAB360), rabbit OLIG2 (Novus Bio; 28667SS).

Generation of Nestin Cre SR mice: Nestin Cre (conditional deletion of SR) mice were generated by breeding SR flox mice (Basu et al., 2009) with nestin cre mice obtained from Jackson labs (number 003771) to generate nestin cre SR flox $^{+/-}$ or nestin cre (-) SR flox $^{+/-}$. The nestin cre (+) SR flox$^{+/-}$ mice were then bred with SR flox mice to obtain nestin cre SR flox/flox. From the litters obtained and after genotyping (Transnetyx Inc) nestin cre SR flox/flox mice were then bred with SR flox mice to obtain nestin cre SR flox/flox or SR flox/flox mice. The nestin cre SR flox/flox mice were used in experiments along with SR flox/flox mice as controls. All mice were age matched and genotyped before use in experiments (Giusti et al., 2014). *Note:* Flox and SR Flox refer to SR $^{flox/flox}$ and Nestin Cre to nestin-cre+ (conditional deletion of SR) mice in this study.

BrdU (Bromo deoxy Uridine) labeling: Eight weeks old WT and age matched SR$^{-/-}$ mice (and SR $^{flox/flox}$, nestin-cre+ mice) were kept in a cage and administered 1 mg/ml BrdU (Bromo deoxy Uridine) in the water by means of a water bottle (*ad libitum*) contained within the cage for 14 days. The water was changed after 7 days with fresh solution of BrdU. On day 13 the mice were given a single i.p. injection of 200 μl BrdU (5 mg/ml) and the brains harvested after 18 h following euthanasia. The brains were perfused with 4 % PFA in PBS. The brains were sectioned after paraffin embedding. BrdU incorporation in the brain was detected using anti BrdU antibody staining by IHC with antigen retrieval at 60°C for 10 min. The imaging was performed using laser scanning confocal microscopy and a *z* stack obtained. The number of BrdU positive cells were counted in each section and quantified (Doetsch et al., 1999).

Micro dissection of adult mouse brain SVZ: The mice brain was dissected and removed following euthanasia and kept in a sterile petri dish containing sterile PBS. The petri dish containing the individual brain was placed under a dissecting microscope with light source at low magnification on the ventral surface and using fine forceps, the olfactory bulbs were removed by holding the cerebellum. The brain was then rotated on to the dorsal aspect and using a sterile blade a coronal cut was made at the level of the optic chiasm. To micro dissect the SVZ, the rostral portion of the brain was positioned to face the cut coronal section upwards. The microscope was focused to a higher magnification. The septum was discarded using fine curved forceps. The SVZ (thin tissue layer adjacent to the ventricle) was dissected by placing the tip of a fine curved forceps in the lateral corner of the ventricle adjacent to the corpus callosum and the other tip approximately 1 mm into the tissue immediately adjacent to the ventricle. The tissue was gently pressed down with the forceps and the triangular piece of tissue removed. The dissected SVZ was placed on a petri dish on ice. A total of 5-10 mice SVZ regions per genotype were pooled in each isolation (Walker and Kempermann, 2014).

Adherent monolayer stem cell culture: The neural stem cell adherent monolayer culture system is a valuable tool for determining the proliferative and differentiative potential of adult neural stem cells *in vitro*. The adherent monolayer cultures comprise mostly homogenous population of precursor cells and are useful for following the differentiation process in single cells. The SVZ was carefully dissected from WT, SR$^{-/-}$, SR $^{flox/flox}$ and nestin-cre+ SR mice brains as per the method in (Walker and Kempermann, 2014). The protocol for coating the 96 well and 24 well plate was followed exactly as mentioned. Differentiation of precursor cells in adherent monolayer cultures was followed as per Walker *et al* protocol (Walker and Kempermann, 2014).

Neuroblast Assay: Neuroblasts (Type A cells) were visualized after plating the cells obtained from dissociation of adherent monolayer cultures (mentioned above) following accutase treatment. The dissociated monolayer cells were plated in a 15 μ 24 well plate at 2-3 X 10^5 cells/ml in complete NSC medium supplemented with 20 ng/ml EGF and 10 ng/ml b-FGF. The plated cells were incubated at 37°C incubator for 3-4 days to achieve 75-80 % confluence. Differentiation was induced by gradually replacing media with less growth factors (10 ng/ml b-FGF and 5 ng/ml EGF to no growth factors). The media was subsequently replaced with no growth factors. The differentiated cells (4-5 days post induction) were fixed with 4 % PFA in PBS and immunostained for PSA-NCAM (marker for neuroblasts), β-III tubulin (neuronal marker) and NeuroD1 (neuronal maturation). DAPI was used as a nuclear stain in the mounting media. The cells were visualized under a fluorescence microscope and positively stained cells were counted in each high-powered field and neuroblasts quantified (Azari and Reynolds, 2016; Azari et al., 2012).

Neural Stem Cell Immunocytochemistry: Staining of NSC's for expression of different markers was performed in a 15 μ 24 well plate (thin glass bottom; Ibidi; #82406). The cells were washed once with 0.5 ml PBS. The cells were fixed with 4 % PFA in PBS for 20 min at RT. After fixation, the cells were washed once in PBS. The cells were then blocked in 0.5 % triton X-100 in PBS for 60 min at RT. Following the blocking step, the cells were incubated with the different primary antibodies (1:500-1:1000 dilution) in blocking buffer for 60 min at RT. After incubation, the cells washed 3 times in PBS. The cells were incubated with anti-mouse or anti-rabbit Alexa fluor secondary antibodies (1:1000-1:2000 dilution) in blocking buffer for 30 min at RT in the dark. The cells were washed 3 times in PBS. A drop of the mounting medium (ProLong Diamond Antifade Mountant with DAPI; Invitrogen; #P36962) was added to each well and a circular coverslip placed gently in the well. The coverslip was tapped gently to remove any air bubbles. The plate was wrapped in foil and allowed to dry at 4°C in the dark. The cells were imaged using a fluorescence microscope.

Mouse FASN ELISA: Mouse FASN (fatty acid synthase) expression in mice brain and SVZ region was measured quantitatively using mouse FASN ELISA kit (CUSABIO cat# CSB-EL008435MO). A standard curve was generated from purified mouse FASN as per instructions. Lysates from whole brain and SVZ regions of age matched SR $^{flox/flox}$ and nestin-cre+ mice were homogenized in PBS containing protease inhibitors, sonicated and the harvested supernatant diluted (1:20 v/v) in PBS containing protease inhibitors. Protein concentration was estimated using BCA assay. Equal amounts of protein were added to each well of a 96 well plate in triplicate and the ELISA performed as per manufacturer's instructions. The absorbance at 450 nm was correlated to the amount of FASN (in pg/ml) in the sample based on a FASN standard curve.

Mouse Malonyl CoA ELISA: Estimation of mouse malonyl CoA in SVZ lysates was measured quantitatively using mouse malonyl CoA ELISA kit (CUSABIO cat# CSB-E12896m). A standard curve of purified malonyl CoA was generated as per manufacturer's instructions in the concentration range of 0-10 ng/ml. SVZ lysates from age matched SR $^{flox/flox}$ and nestin-cre+ mice were prepared in PBS containing protease inhibitors. The stock lysate was diluted 1:500 in PBS containing protease inhibitors and protein concentration estimated using BCA assay. Equal amounts of protein were added to each well of the 96 well ELISA plate in triplicate. The ELISA was performed as per the instructions in the manufacturer's catalog. Absorbance was read in a microplate reader at 450 nm and background correction of the wells was done at 540 nm. The amount of malonyl CoA (ng/ml) in the SVZ was estimated from the standard curve.

Quantitative lipidomic analysis: Quantitative lipidomic analysis on SVZ tissue from SR $^{flox/flox}$ and nestin- cre+ mice (N=5-8 mice pooled per set per genotype; N=2 sets per genotype) and run in triplicate was done at The Metabolomics Innovation Center (TMIC) University of Alberta Canada. The analysis was performed under the four different steps listed below.

Lipid Extraction. The extraction was performed strictly following the SOP established based on a modified Folch liquid-liquid extraction protocol. Each sample was extracted in duplicate. The mass of each sample aliquot (5.0 to 6.8 mg) was employed as a normalization factor for the extraction solvents and reagents. Briefly, each aliquot of SVZ brain tissue was vortexed and homogenized with 1.0 µL of

internal standard solution / mg of sample and 33.3 µL/mg of methanol, followed by extraction with 65.7 µL/mg of dichloromethane. A clean-up step was performed with 23.6 µL/mg of water. Samples were allowed to equilibrate at room temperature for 10 min and centrifuged at 16,000 g for 10 min at 4°C. An aliquot of the organic layer was evaporated to dryness with a nitrogen blowdown evaporator. The residue was immediately re-suspended in 7.0 µL/mg of NovaMT MixB, vortexed for 1 min, and diluted with 63.0 µL/mg of NovaMT MixA (see below). A pooled mixture of the extracts of both samples was prepared for quality control.

LC-MS Analysis. The LC-MS analyses were performed by strictly following the SOP in both positive and negative ionization with extraction duplicates. A total of 12 sample injections (2 samples with extraction duplicates and injection triplicates per genotype) and 10 quality control injections (a pooled mixture of the extracts of both samples) were performed in each ionization polarity. MS/MS spectra were acquired for all samples for identification. Parameters used for data acquisition are described below.

Instrument:	Thermo Vanquish UHPLC linked to Bruker Impact II QTOF Mass Spectrometer
Column:	Waters Acquity CSH C18 column, 1.7 µm.
MPA:	NovaMT MixA
MPB:	NovaMT MixB
Gradient:	NovaMT 26-min-gradient
Flow Rate:	250 µL/min.
Injection Volume:	5.0 µL for positive ionization and 10.0 µL for negative ionization
Column Oven Temperature:	42 °C
Mass Range:	m/z 150-1500
MS/MS Collision Energies:	10-80 eV

Data Processing. LC-MS data from 22 injections were independently processed in positive and negative ionization. Lipid features were extracted and aligned using NovaMT LipidScreener. The data acquired in positive and negative ionization from each sample extraction were combined, i.e. the detected features from all samples were merged into one feature-intensity table. Missing values were substituted by the average intensity of the sample group for features detected in at least 50% of injections within the group (Nestin Cre, SR Flox and QC); or by the global minimum for all sample and QC injections for features detected in less than 50% of injections within the group. Parameters used for data processing are below.

Minimum Intensity Cut-off:	3000 cts for negative ionization; 3000 cts for positive ionization
Minimum Peak Length:	6 spectra
Retention Time Tolerance	5 seconds
Mass Tolerance:	5 mDa
Feature Filtering:	Detection for ≥80% of injections in at least one sample group (Nes Cre, SRFlox and QC)

Lipid Identification. A three-tier identification approach based on MS/MS identification and MS match was employed for lipid identification. The parameters used for identification are described below.

Tier 1 (MS/MS identification):	MS/MS match score ≥ 500; precursor m/z error ≤ 5 mDa
Tier 2 (MS/MS identification):	MS/MS match score ≥ 100; precursor m/z error ≤ 5 mDa
Tier 3 (MS match):	Mass match with m/z error ≤ 5 mDa

After tier 3 identification, a six-tier filtering and scoring approach embedded in NovaMT LipidScreener was employed to restrict the number of matches and select the best identification option to determine the

lipid sub-classes for normalization. Data normalization was performed by using a set of 14 deuterated internal standards belonging to different lipid classes. The positively and putatively identified lipids were matched to one of the 14 internal standards according to lipid class similarity and expected retention time range for each class. Intensity ratios, i.e., intensity of each lipid divided by intensity of the matched internal standard, were calculated for normalization. Statistical analysis was performed with MetaboAnalyst 5.0 (https://www.metaboanalyst.ca/). Non-informative features (i.e., internal standards) and features with low repeatability (RSD >20% for QC injections) were filtered out. The dataset was further normalized by auto-scaling and to the median intensity. Finally, the normalized and auto-scaled features were used for statistical analysis.

Analysis of Gene expression: RNA was isolated from SVZ of WT and $SR^{-/-}$, $SR^{flox/flox}$ and nestin-cre+ mice using RNA isolation kit (Ambion). Gene expression studies related to glucose homeostasis and pancreas development were performed using the SYBR green method. cDNA synthesis was performed using High Capacity cDNA synthesis kit (Applied Biosystems). 100 ng of synthesized cDNA was used in each well of a 96 well 0.1 ml MicroAmp PCR plate (Applied Biosystems) along with SYBR Green master mix, nuclease free water and gene specific primers (1 μM final concentration) in a total volume of 10 μl. 18S rRNA was used as a housekeeping gene and non-template control was added in each plate as a control. Samples were run in triplicate. The PCR was run on an ABI Step One Plus instrument. The raw data obtained was analyzed on Step One data analysis software and mean C_T values obtained. ΔC_T and $\Delta\Delta C_T$ were calculated and fold change in gene expression obtained from $2^{exp\text{-}\Delta\Delta CT}$. The primer sequences spanning exon-exon boundaries for qPCR using SYBR Green are listed in Table S3.

Immunohistochemistry: Immunohistochemical experiments were performed on WT, $SR^{-/-}$, SR flox and nestin cre mice brain coronal and saggital sections. Briefly, the mice were euthanized by CO_2 narcosis and perfused with 4% paraformaldehyde (PFA) in PBS by cardiac puncture technique. The brain was removed and incubated at 4°C for 48 h in 4% PFA in PBS with gentle shaking. The tissue was paraffin embedded at the Johns Hopkins Oncology Core Services and sectioned at 4 μ thickness. The sections were de paraffinized using Histoclear (5 min X 2) followed by sequential incubations in absolute alcohol (5 min X 2), 95% alcohol (5 min X 2) and PBS (10 min X 2). The sections were permeabilized in 0.5% Triton X-100 in PBS for 10 min. Antigen retrieval was performed in 10 mM citrate buffer + 0.05% Tween at 60°C for 10 minutes. The sections were cooled on ice for 15 min. The sections were blocked with 1% BSA in PBS for 30 min. The sections were incubated with primary antibody (1:500 dilution in blocking buffer) a 4°C overnight. The slides were washed in PBS (10 min X 2) followed by incubation with secondary antibody (1:1000 dilution in blocking buffer) at RT for 30 min and protected from light. The sections were washed in PBS (10 min X 2). The slides were then cover slipped with mounting medium containing DAPI and edges sealed with transparent nail polish. The slides were allowed to dry at 4°C and observed using confocal microscopy.

Confocal Microscopy: Fluorescently stained mice brains SVZ sections from age matched WT, $SR^{-/-}$, $SR^{flox/flox}$ and nestin-cre+ mice were imaged on LSM 780 and LSM 810 confocal microscope (Zeiss) at 10X and 20X magnification at the microscopy core facility at Johns Hopkins. Images were acquired at different high powered fields in each section. All settings and parameters were kept constant during image acquisition. Scale bars were added to each image using Zen black software.

Rescue in monolayer adherent cultures: Rescue experiments in adherent monolayer cultures were performed by isolating NSC's from the SVZ of age matched adult WT, $SR^{-/-}$, $SR^{flox/flox}$ and nestin-cre+ mice. Following isolation based on protocol mentioned above, the cells were plated in 500 μl of growth factor media in coated 24 well plates. After 24 h, the media was replaced completely in each well with fresh media containing either an equimolar mixture of L and D-serine (100 μM) or individually with L-serine (0.6 mM) and D-serine (0.1 mM). Control cells did not receive any L or D-serine. The media with L and D-serine were replaced every 2-3 days (50 % volume in each well). Both L and D serine were made fresh on the day of addition. The cells were grown in culture for 7-10 days following which differentiation was induced by gradual removal of growth factors as mentioned in (Walker and Kempermann, 2014). All media added to rescue group of cells contained freshly prepared L and D-serine. The cells were harvested 3-4 days after induction of differentiation at which time neuroblasts were present. For

immunocytochemistry, the cells were fixed, permeabilized and stained in the 24 well plate. The cells were covered with a coverslip in the well following staining with a drop of antifade mounting medium and stored in the dark at 4°C.

Western blot: Whole brain and SVZ lysates were run on a 1 mm 4-12% Bis-Tris gel (Novex Life Technologies; Thermo Fisher) with MES SDS running buffer (Invitrogen; #NP0002-02) initially at 75 V and then at 120 V. The samples were then transferred to a pre-wet immobilon PVDF transfer membrane (Merck Millipore Ltd; Pore Size 0.45 μm) and sandwiched between wet filter paper and cassette holder. The entire apparatus was placed in a wet transfer apparatus (Bio-Rad) and run at 90 V for 90 min on ice. After transfer, the membrane was removed and incubated in blocking buffer containing Tris buffered saline + Tween 20 (TBS-T) containing 5% BSA for 30 minutes at room temperature (RT). The membrane was incubated on a shaker with the respective primary antibody at 1:1000 dilution in blocking buffer overnight at 4°C. After overnight incubation, the membrane was rinsed 3 times with TBS-T and washed in TBS-T at RT for 15 minutes per wash. The membrane was washed a total of 4 times. After washing, the membrane was incubated with HRP conjugated secondary antibody (IgG; mouse or rabbit) (GE Healthcare UK) at 1:5000 dilution in blocking buffer and incubated at RT with shaking for 1 h. After incubation with secondary antibody, the membrane was washed 4 times with TBS-T. The duration of each wash was 15 min. After the last wash, the membrane was incubated with Enhanced Chemiluminescent (ECL) reagent (Thermo Scientific; Super Signal West Pico Plus Peroxide solution and Luminol enhancer solution in a 1:1 (v/v) for 5 min in the dark. The excess ECL reagent was removed using a kimwipe and the membrane was placed in between a plastic sheet and in a cassette holder and developed on an 8" X 10" Ultra Cruz autoradiography film (Santa Cruz Biotechnology) in a developer.

Time spent sniffing novel odor. Mouse olfactory behavior was tested in age matched WT and $SR^{-/-}$ mice (N=20-25 per group) were collected and brought to the behavior suite and the mice placed in clean cages with new bedding. The mice were placed in an adjacent room before testing and acclimatized in their new cage for 5 minutes. The new cage had bedding 2-2.5 inches deep. The mice were prepared as mentioned above for this test. Using two disposable pipettes two drops of vanilla extract were placed on one side of the cage and two drops of water were placed on the opposite side of the cage. This eliminates the confounding principle of investigating a novel "object" versus a novel odor. The mice are timed for 2 minutes and recorded for the amount of time it spends sniffing the vanilla extract within the allotted 2 minutes. The data are recorded if the mouse is within 1.5 inches of the placed vanilla extract. The mice are then returned to their original cages. The data were compared between the groups.

Blood Glucose Estimation. Blood glucose level was monitored by tail bleeding immediately before and at indicated times after injection using Contour glucometer (Bayer Co, Japan) and Contour blood glucose test strips (Cat#7097C; Ascensia Diabetes care Inc, NJ). Blood glucose measurements were obtained from tail veins at indicated time points post injection. A small drop of blood from the tail was placed on a new glucose strip each time, inserted into the glucometer and value recorded.

Insulin ELISA: Quantitative estimation of insulin from brain homogenates and SVZ (following microdissection) of age matched WT, $SR^{-/-}$, $SR^{flox/flox}$ and nestin-cre+ mice was performed using the Ultra Sensitive Mouse Insulin ELISA Kit (Cat# 90080; Crystal Chem). The protocol was followed exactly as mentioned for the low range assay. Standard curve for insulin was developed prior to the actual experiment (low range). Each individual sample was done in quadruplicate. The samples were pooled from N=4-10 mice per genotype and analyzed. The absorbance was read at 450 nm in a 96 well plate reader and also at 630 nm and data plotted after correction at 630 nm.

Protein-protein Interaction Network Analysis. The search tool for retrieval of interacting genes (STRING) (https://string-db.org) database was applied to predict functional interactions of proteins. To seek potential interactions between differentially expressed genes, the STRING tool was employed with k means clustering. Edges between clusters are shown in dashed lines. Interactions within a cluster is shown in solid lines. Text mining, databases, and co-expression as well as species limited to *Homo sapiens* and *Mus musculus* were applied to construct the protein-protein interaction networks (Szklarczyk D et al).

Statistics: Statistical tests were computed using KaleidaGraph (Synergy Software, Reading PA). Data are represented as mean ± SD. Unpaired student's t test was used for pairwise comparison with a fixed control condition. For multiple pairwise comparisons with different control and treatment conditions, one-way ANOVA analysis followed by Tukey's post hoc test was used. Values with $p < 0.05$ were considered significant.

Key Resources Table

REAGENT or RESOURCE	SOURCE	IDENTIFIER
Antibodies		
Rabbit anti Ki67 antibody	Novus Bio	NB500-170SS
Rabbit anti FASN antibody	Bethyl Labs	A301-324A-T
Mouse anti PSA-NCAM antibody	DSHB Iowa	5A5-c
Mouse anti Spot14 antibody	Santacruz Biotechnology	sc-137178
Rabbit anti MCM2 antibody	Bethyl Labs	IHC-00009-T
Mouse anti BrdU antibody	Sigma	B8434-25
Mouse anti CD24 antibody	eBioscience	14-0242-82
Rabbit anti Serine Racemase antibody D5V9Z	Cell Signaling Technology	#29798
Rabbit anti Prominin antibody	Millipore	ZRB1013-25
Rabbit anti NeuN antibody	Cell Signaling Technology	D4G40
Mouse anti β-III tubulin antibody	R&D Systems	MAB1195-SP
Mouse anti GFAP antibody	Millipore	MAB360
Rabbit anti Olig2 antibody	Novus Bio	28667SS
Rabbit anti Akt antibody	Cell Signaling Technology	9272S
Rabbit anti phospho-Akt (S473) antibody	Cell Signaling Technology	4060S
Rabbit β-actin antibody	ABClonal	NO:AC026
Goat anti mouse Alexa 547 secondary antibody	Invitrogen	R37121
Goat anti rabbit Alexa 488 secondary antibody	Abcam	ab150077
Bacterial and virus strains		

N/A		
Biological samples		
N/A		
Chemicals, peptides, and recombinant proteins		
L-serine	Sigma	S4500
D-serine	Sigma	S4250
Ascensia Contour Blood Glucose meter	Bayer Healthcare LLC	7151B
Contour Blood Glucose test strips	Ascensia Diabetes Care	7097C
Critical commercial assays		
Mouse FASN ELISA Kit	CUSABIO	CSB-EL008435MO
Mouse Malonyl CoA ELISA Kit	CUSABIO	CSB-E12896m
Mouse Insulin ELISA Kit	Crystal Chem	#90080
Deposited data		
N/A		
Experimental models: Cell lines		
N/A		
Experimental models: Organisms/strains		
$SR^{-/-}$ mouse (Serine Racemase knock out mouse)	Basu et al; Molecular Psychiatry 2009	Joe Coyle, Harvard Medical School
WT mouse C57 BL/6	Jackson Labs	#000664
$SR^{flox/flox}$ mice		Joe Coyle, Harvard Medical School

Nestin Cre mice (background)	Jackson Labs	003771
Nestin-Cre+ mice	This paper	
Oligonucleotides		
Spot14, Citrate Lyase, Cpt1a, Mig12, Acc primers	Knobloch et al; Nature 2013; Table 3, this paper.	
Mouse PSPH qPCR primer pair	Sino Biological	MP201727
Mouse PHGDH qPCR primer pair	Sino Biological	MP201627
HACoA primer	Table 3, this paper	
ECH1 primer	Table 3, this paper	
Recombinant DNA		
N/A		
Software and algorithms		
Zen Black	Zeiss	https://www.zeiss.com/microscopy/us/products/microscope-software/zen.html
Image J	NIH	https://imagej.nih.gov/ij
KaleidaGraph v4.1	Synergy Software	https://www.synergy.com

Slidebook 6	3i-Intelligent Imaging Innovations	https://www.intelligent-imaging.com/slidebook

Supplemental References

Basu, A.C., Tsai, G.E., Ma, C.L., Ehmsen, J.T., Mustafa, A.K., Han, L., Jiang, Z.I., Benneyworth, M.A., Froimowitz, M.P., Lange, N.*, et al.* (2009). Targeted disruption of serine racemase affects glutamatergic neurotransmission and behavior. Mol Psychiatry *14*, 719-727.

Giusti, S.A., Vercelli, C.A., Vogl, A.M., Kolarz, A.W., Pino, N.S., Deussing, J.M., and Refojo, D. (2014). Behavioral phenotyping of Nestin-Cre mice: implications for genetic mouse models of psychiatric disorders. J Psychiatr Res *55*, 87-95.

Doetsch, F., Caille, I., Lim, D.A., Garcia-Verdugo, J.M., and Alvarez-Buylla, A. (1999). Subventricular zone astrocytes are neural stem cells in the adult mammalian brain. Cell *97*, 703-716.

Walker, T.L., and Kempermann, G. (2014). One mouse, two cultures: isolation and culture of adult neural stem cells from the two neurogenic zones of individual mice. J Vis Exp, e51225.

Azari, H., and Reynolds, B.A. (2016). In Vitro Models for Neurogenesis. Cold Spring Harb Perspect Biol *8*.

Azari, H., Sharififar, S., Fortin, J.M., and Reynolds, B.A. (2012). The neuroblast assay: an assay for the generation and enrichment of neuronal progenitor cells from differentiating neural stem cell progeny using flow cytometry. J Vis Exp.

Szklarczyk D, Franceschini A, Wyder S, Forslund K, Heller D, Huerta-Cepas J, et al. (2015). STRING v10: protein-protein interaction networks, integrated over the tree of life. Nucleic Acids Res, 43:D447–52.

Pircs, K., Petri, R., Jakobsson, J. (2018). Crosstalk between MicroRNAs and Autophagy in Adult Neurogenesis: Implications for Neurodegenerative Disorders. Brain Plast 3(2),195-203.